Check for updates

ChemMedChem

Chemistry Europe
European Chemical Societies Publishing

Accepted Article

Title: A New Series of Ferulic Acid Amides Reveals an Unexpected Peroxiredoxin 1 Inhibition Activity With In Vivo Antidiabetic and Hypolipidemic Effects

Authors: Sabina Yasmin, Carmen Cerchia, Vishnu Nayak Badavath, Antonio Laghezza, Fabrizio Dal Piaz, Susanta K. Mondal, Özlem Atlı, Merve Baysal, Sankaran Vadivelan, Shankar S, Mohd Usman Mohd Siddique, Ashok Kumar Pattnaik, Ravi Pratap Singh, Fulvio Loiodice, Venkatesan Jayaprakash, and Antonio Lavecchia

This manuscript has been accepted after peer review and appears as an Accepted Article online prior to editing, proofing, and formal publication of the final Version of Record (VoR). This work is currently citable by using the Digital Object Identifier (DOI) given below. The VoR will be published online in Early View as soon as possible and may be different to this Accepted Article as a result of editing. Readers should obtain the VoR from the journal website shown below when it is published to ensure accuracy of information. The authors are responsible for the content of this Accepted Article.

To be cited as: *ChemMedChem* 10.1002/cmdc.202000564

Link to VoR: https://doi.org/10.1002/cmdc.202000564

WILEY-VCH

FULL PAPER WILEY-VCH

A New Series of Ferulic Acid Amides Reveals an Unexpected Peroxiredoxin 1 Inhibition Activity With In Vivo Antidiabetic and Hypolipidemic Effects

Sabina Yasmin,[a,b],+ Carmen Cerchia,[c],+ Vishnu Nayak Badavath,[a] Antonio Laghezza,[d] Fabrizio Dal Piaz,[e] Susanta K. Mondal,[f] Özlem Atlı,[g] Merve Baysal,[g] Sankaran Vadivelan, [h] Shankar S,[h] Mohd Usman Mohd Siddique,[a,j] Ashok Kumar Pattnaik,[a] Ravi Pratap Singh, [a] Fulvio Loiodice,*[d] Venkatesan Jayaprakash,* [a] and Antonio Lavecchia*[c]

[a] Dr. S. Yasmin, + Dr. V. N. Badavath, Dr. M. U. M. Siddique, Dr. A. K. Pattnaik, Dr. R. P. Singh, Dr. V. Jayaprakash
Department of Pharmaceutical Sciences & Technology,
Birla Institute of Technology
Mesra, Ranchi, Jharkhand 835 215, India
E-mail: drvenkatesanj@gmail.com

[b] Dr. S. Yasmin+
Department of Pharmaceutical Chemistry
College of Pharmacy, King Khalid University
Abha, 61441, Saudi Arabia

[c] Dr. C. Cerchia,+ Prof. A. Lavecchia
Department of Pharmacy, "Drug Discovery" Laboratory
University of Napoli "Federico II"
Via D. Montesano, 49, 80131 Napoli, Italy
E-mail: antonio.lavecchia@unina.it

[d] Dr. A. Laghezza, Prof. F. Loiodice
Department of Pharmacy & Drug Sciences
University of Bari "Aldo Moro"
via Orabona 4, 70125 Bari, Italy
E-mail: fulvio.loiodice@uniba.it

[e] Prof. F. Dal Piaz
Department of Pharmacy
University of Salerno
Via Giovanni Paolo II, 132, 84084, Fisciano, Italy

[f] Dr. S. K. Mondal
TCG Lifesciences Ltd
Block-EP & GP, BIPL, Tower-B, Saltlake, Sector-V, Kolkata, 700091 West Bengal, India

[g] Dr. Ö. Atlı, Dr. M. Baysal
Department of Pharmaceutical Toxicology
Faculty of Pharmacy, Anadolu University
Yunus Emre Kampüsü, 26470 Eskişehir, Turkey

[h] Dr. Ö. Atlı, Dr. M. Baysal
Department of Pharmaceutical Toxicology
Faculty of Pharmacy, Anadolu University
Yunus Emre Kampüsü, 26470 Eskişehir, Turkey

[i] Dr. S. Vadivelan, Dr. S. S
Eurofins Advinus Limited, 21 & 22
Peenya Industrial Area, 560058 Bengaluru, India

[j] Dr. M. U. M. Siddique
Department of Pharmaceutical Chemistry
Shri Vile Parle Kelavani Mandal's Institute of Pharmacy
Dhule, 424001 Maharashtra, India

+These authors contributed equally to this work

Supporting Information for this article is given via a link at the end of the document.

Abstract: Insulin resistance is a major pathophysiological feature in the development of type 2 diabetes (T2DM). Ferulic acid is known for attenuating the insulin resistance and reducing the blood glucose in T2DM rats. In this work, we designed and synthesized a library of new ferulic acid amides (FAA), which could be considered as ring opening derivatives of the antidiabetic PPARγ agonists Thiazolidinediones (TZDs). However, since these compounds displayed weak PPAR transactivation capacity, we employed a proteomics approach to unravel their molecular target(s) and identified the peroxiredoxin 1 (PRDX1) as a direct binding target of FAAs. Interestingly, PRDX1, a protein with antioxidant and chaperone activity, has been implied in the development of T2DM by inducing hepatic insulin resistance. SPR, mass spectrometry-based studies, docking experiments and in vitro inhibition assay confirmed that compounds **VIe** and **VIf** bound PRDX1 and induced a dose-dependent inhibition. Furthermore, **VIe** and **VIf** significantly improved hyperglycemia and hyperlipidemia in streptozotocin-nicotinamide (STZ-NA)-induced diabetic rats as confirmed by histopathological examinations. These results provide guidance for developing the current FAAs as new potential antidiabetic agents.

Accepted Manuscript

This article is protected by copyright. All rights reserved.

Introduction

Type 2 diabetes mellitus (T2DM) is a chronic and common lifestyle disease that is caused by complex interactions between multiple susceptibility genes and environmental factors. It is characterized by high levels of blood glucose (hyperglycemia) due to a defective insulin signaling in adipose tissue, liver and muscle cells. This phenomenon, that is called insulin resistance, is usually associated with other cardiovascular risk factors such as hypertension, obesity, dyslipidemia, and unhealthy lifestyles (e.g., inadequate diet, excessive lipids accumulation, sedentarism).[1] The global incidence of this disease is estimated to be more than 180 million people across the world and expected to increase to 366 million in 2030.[2] Development of T2DM can be prevented or at least delayed by appropriate lifestyle changes or the use of therapeutic agents. However, most of the drugs used show lack of effectiveness or trigger unexpected side effects, forcing patients to discontinue the treatment.[3] For this reason, as well as for the high social impact of diabetes, there is a need to search for new potent anti-diabetic agents with better pharmacological profiles.

In the last decades, an increasing number of studies revealed that many natural substances modulate the insulin resistance signaling, thereby acting on carbohydrates and/or lipids metabolism.[4] Interestingly, several of these biologically active substances are able to influence lipid and glucose homeostasis without showing adverse effects. Thus, it is general opinion that they could be used as new drugs to treat T2DM or, alternatively, could provide novel scaffolds to obtain new and more specific antidiabetic drugs. Ferulic acid (Figure 1) is a natural phenolic compound of some Chinese medicinal herbs, such as *Angelica sinensis*, *Cimicifuga racemosa* and *Ligusticum chuangxiong*.[5] This compound and its derivatives exhibit a wide range of therapeutic effects with applications including anticancer, cardioprotective, neuroprotective, anti-inflammatory and, most importantly, antidiabetic activities.[6] In 2003, Nomura et al.[7] reported that ferulic acid amide (FAA) derivatives exhibited their stimulatory abilities on insulin secretion in rat pancreatic RIN-5F cells. Later, new reports were published on antioxidant activity and hypoglycemic effect of ferulic acid in STZ-induced diabetic mice and KKAy mice, and its synergistic interaction with commercially available antidiabetics in STZ-induced diabetic rats.[8] Therefore, in our continuing interest to develop new compounds for antidiabetic drug discovery, here we undertook the design and synthesis of the series of FAA derivatives reported in Figure 1. In these compounds, also, we introduced an acetanilido group on the phenolic function in order to protect it towards the conjugation processes so increasing the metabolic stability and the following drug persistence; at the same time, we wanted to explore the effects on activity due to new possible interactions with the hypothetical target through the presence of additional hydrogen bond donors and acceptors in this region of the molecule. This design led to compounds that could be considered, at first glance, as ring opening derivatives of Thiazolidinediones (TZDs), a class of drugs that are clinically used for treatment of T2DM. The biological target of TZDs is represented by PPARγ, which is a known ligand-dependent transcription factor belonging to the nuclear receptor superfamily and modulating, together with the other two subtypes PPARα and PPARδ, the genes involved in lipid and glucose metabolism.[9] For this reason, all the compounds were analyzed for their in vitro activity towards PPARα, PPARγ and PPARδ by using GAL4-PPAR transactivation assay. However, no PPAR transactivation activity was observed in response to any ligand even though surface plasmon resonance (SPR) measurements indicated that FAAs bind directly to PPARγ with moderate binding affinity.

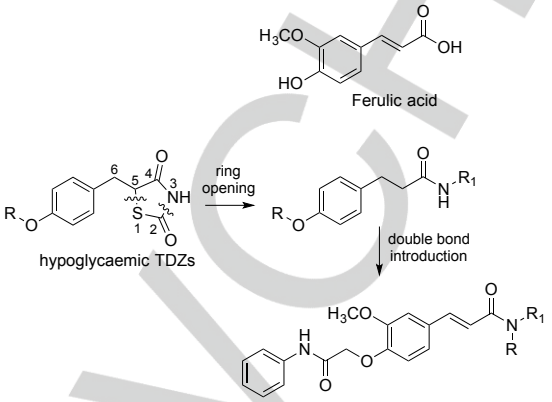

VIa R = H; R_1 = C_6H_5

VIb R = H; R_1 = CH_2-C_6H_5

VIc R = H; R_1 = $(CH_2)_2$-C_6H_5

VId R = H; R_1 = cy-C_6H_{11}

VIe R, R_1 = -$(CH_2)_4$-

VIf R, R_1 = -$(CH_2)_2$-O-$(CH_2)_2$-

VIg R, R_1 = -$(CH_2)_5$-

VIh R = H; R_1 = CH_3

VIi R = H; R_1 = C_2H_5

VIj R = H; R_1 = C_4H_9

VIk R = H; R_1 = $CH(CH_3)_2$

VIl R = R_1 = CH_3

VIm R = R_1 = C_2H_5

Figure 1. Correlation between the hypoglycaemic TZDs and the FAA derivatives **VIa-m**.

Nonetheless, the intriguing therapeutic effects shown by ferulic acid and its derivatives prompted us to unravel the molecular target(s) of our FAAs library by using a proteomics approach. In this regard, we used the Drug Affinity Responsive Target Stability (DARTS) assay that detects the interaction between the target protein and a small molecule by measuring resistance to proteolysis,[10] and identified the peroxiredoxin 1 protein (PRDX1) as a putative target of compounds **VIe** and **VIf**, chosen as representative examples of the series. Interestingly, some recent studies suggest that this protein, which is a member of PRDX family capable to prevent oxidative damage to proteins by serving as a chaperone, could be potentially involved in the development of diabetes mellitus by inducing hepatic insulin resistance.[11] SPR analysis, mass spectrometry-based studies and in vitro inhibition assays confirmed the direct interaction between **VIe** and **VIf** and PRDX1 and showed a dose-dependent inhibition of the enzyme activity. Docking studies were also carried out to gain insights into the possible binding mode of FAA derivatives and to elucidate the molecular mechanism of inhibition. Furthermore, **VIe** and **VIf** were tested in in vitro preclinical profiling assays to evaluate their apparent pharmaceutical properties (LogD, liver microsomal stability ($t_{1/2}$), and apparent permeability). A pharmacokinetic study of **VIe** and **VIf** was also carried out in male Sprague-Dawley rats following

This article is protected by copyright. All rights reserved.

Accepted Manuscript

intravenous and oral administration. Finally, we investigated the antidiabetic effects of **VIe** and **VIf** and found that treatment with FAAs could ameliorate metabolic parameters and hyperlipidemia in streptozotocin-nicotinamide (STZ-NA)-induced diabetic rats, as well as preserve the normal histological appearance of pancreatic islets and liver. Taken together, our findings provide molecular evidence of a new series of compounds that could represent an alternative and potentially safer way for the treatment of T2DM.

Results and Discussion

Chemistry

In search for novel PPARγ ligands with potential to exhibit strong glucose-lowering properties without provoking side effects associated with full PPARγ activation, we designed and synthesized a series of simplified FAA derivatives resulting from TZD ring opening and introduction of a double bond at position C5-C6 of the classical hypoglycaemic TZDs (derivatives **VIa-m** in Figure 1). In order to study initial structure-activity relationships (SARs), the methoxy group of ferulic acid was maintained, while the phenolic group was replaced by an anilido substituent with the aim to mimic the alkoxy chain of TZDs. In this way, also, we protected it towards the conjugation processes so increasing the metabolic stability and the following drug persistence; at the same time, the introduction of this group allowed to explore the effects on activity due to new possible interactions with the hypothetical target through the presence of additional hydrogen bond donors and acceptors in this part of the molecule.

All FAA derivatives were prepared according to the reactions outlined in Figure 2. Ferulic acid (**I**) was prepared by reaction between vanillin and malonic acid using toluene as a solvent in the presence of pyridine and aniline. Protection of the phenol group of ferulic acid was carried out by reaction with acetic anhydride and 4-dimethylaminopyridine (DMAP) to provide acetylated ferulic acid (**II**), which was transformed into the corresponding acyl chloride **III** by using oxalylchloride and catalytic amount of dimethylformamide in dry dichloromethane at 0-10 °C. **III** was very unstable, so it was promptly amidated by reaction with appropriate amines in dry dichloromethane and triethylamine to provide **IVa-m**. Deprotection of **IVa-m** by reaction with 4% hydrazine hydrate in acetonitrile for 30-35 min at room temperature provided **Va-m**, which were further treated with N-phenyl-chloroacetamide in the presence of potassium carbonate in dimethylformamide for 72-80 h to produce the final compounds **VIa-m**. Known intermediates were confirmed by comparing their points with the literature values and final compounds were characterized by ^{1}H-NMR, ^{13}C-NMR and ESI-MS spectra.

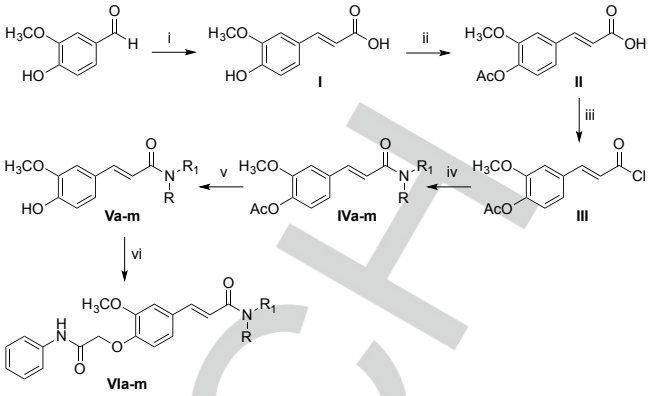

Figure 2. General synthetic route for the title compounds **VIa-m**. Reagents and conditions: (i) $CH_2(COOH)_2$, C_5H_5N, $NH_2C_6H_5$, toluene, reflux, 4 h; (ii) Ac_2O, DMAP, 0-10 ºC; (iii) Dry DCM, DMF, $(COCl)_2$, 0-5 ºC, 2h; (iv) TEA, Dry DCM, R-NHR_1, 0 ºC, 2 h; (v) 4% $NH_2NH_2{\cdot}H_2O$ in CH_3CN, 30-35 min, r.t.; (vi) K_2CO_3, DMF, $C_6H_5NHCOCH_2Cl$, 72-80 h.

Biological studies

First, compounds **VIa-m** were tested for their potential ability to induce transcriptional activation of the human PPARα (hPPARα), PPARγ (hPPARγ), and PPARδ (hPPARδ) subtypes. For this purpose, GAL4-PPAR chimeric receptors were expressed in transiently transfected HepG2 cells according to a previously reported procedure.[12] The activity of these compounds was evaluated at two concentrations (5 μM and 25 μM) and compared with that of the corresponding reference agonists (Wy-14,643 for PPARα, Rosiglitazone for PPARγ, and L-165,041 for PPARδ) whose maximum induction was defined as 100%. Unexpectedly, FAA derivatives did not induce transcriptional activation of any of the three PPAR subtypes. Nonetheless, we decided to evaluate the binding affinity of these compounds for PPARγ. With this aim, we performed a SPR assay monitoring in real time the possible complex formation between compounds **VIa**-**m** and PPARγ ligand binding domain (LBD). The PPARγ protein was immobilized on a sensor chip, and binding responses in RUs were continuously recorded and presented graphically as a function of time in sensorgrams (Figure S1 of Supporting Information).

The equilibrium dissociation constant (K_D) of PPARγ binding to FAAs or Rosiglitazone (as a positive control) was obtained by fitting the sensorgrams with the 1:1 (Langmuir) binding fit model. The affinity (K_D) and rate constants (k_{on}, k_{off}) for PPARγ/**VIa-m** interactions are reported in Table S1 of Supporting Information and compared with the reference ligand Rosiglitazone. Eleven out of thirteen tested FAA derivatives showed binding affinity towards PPARγ even if quite high compound concentrations (from 0.5 to 50 μM) were injected to observe a positive response. Both high k_{off} and low k_{on} values accounted for the weak affinities of FAAs compared with the high-affinity control Rosiglitazone. Using this kinetic analysis, the K_D values for two of the most representative derivatives of the series, **VIe** and **VIf**, were 17.4 and 22.8 μM, respectively. To inspect the potential binding specificity of FAAs for PPARγ, we examined their binding to PPARα and PPARδ LBDs. However, when different concentrations of FAAs flowed through the sensorchip, it was interesting to see no binding affinity against PPARα and PPARδ even at high concentrations (Table S1 of Supporting

This article is protected by copyright. All rights reserved.

Accepted Manuscript

Information), which suggests that FAAs are selective but very weak PPARγ ligands.

DPPH assay

Ferulic acid is a natural compound endowed with well-known antioxidant properties which, at least in part, could explain its antidiabetic activity. For this reason, we decided to evaluate the antioxidant activity of **VIe** and **VIf** by the DPPH assay, a method routinely used for assessment of free radical scavenging potential of an antioxidant molecule. Experiments were carried out by using ferulic acid and gallic acid as reference compounds. However, as expected, **VIe** and **VIf** showed no antioxidant activity in this assay (Table S2 and Figure S2 of Supporting Information) due to the lack of the phenolic function, which is most likely responsible for the antioxidant activity of ferulic acid.

Target(s) Identification of FAA Derivatives VIe and VIf

The identification of further putative targets of compounds **VIe** and **VIf** was attempted using an indirect compound-centered proteomics approach named DARTS (Drug Affinity Responsive Target Stability).[13] It moves from the evidence that susceptibility to proteolysis of a specific protein can be sensibly reduced because of an effective interaction with a partner. DARTS experiments started with the incubation of HepG2 cells with sub-toxic amounts (25 μM) of each compound or with the vehicle (0.1% DMSO in PBS) for 2 h. After that, the cells were lysed under non-denaturing conditions and the obtained proteins underwent to a limited digestion with subtilisin. The resulting partially hydrolyzed protein mixtures were separated by SDS-Page; the gel bands whose intensity showed a higher intensity in the treated samples compared to the controls were in-gel digested and the peptides were analysed by nanoUPLC-hrMS/MS for the subsequent identification of the protein possibly protected from proteolysis by interaction with **VIe** or **VIf**. This procedure was performed in triplicate, and only the proteins emerging from all the experiments were taken into account as possible targets of the two compounds. Eleven different proteins were identified (Table S3 of Supporting Information) and, interestingly, four of them seemed to interact with both the compounds: Hsp90, Hsp70, Annexin 6 and PRDX1. In order to confirm that this result depended on a direct interaction between **VIe** or **VIf** and the proteins, we performed a SPR analysis, injecting different concentration of the two compounds on each of the putative target, singularly immobilized on a sensor chip. Sensorgrams obtained on immobilized Hsp90, Hsp70 or Annexin 6 indicated that neither **VIe** nor **VIf** bound any of these proteins. Conversely, SPR data confirmed that both molecules efficiently interacted with the PRDX1-modified chip (Figure S3A of Supporting Information), and K_Ds of 143 ± 28 nM and 128 ± 16 nM were measured for **VIe** and **VIf**, respectively. On these bases, we used a commercially available assay kit (2-Cys-Peroxiredoxin Activity Assay Kit - Redoxica) to evaluate whether this interaction affected PRDX1 activity. The results indicated that both **VIe** and **VIf** inhibited the enzyme in a concentration-dependent manner (Figure S3B of Supporting Information); also in this case, as for the SPR experiments, similar results were obtained for the two molecules and an apparent IC_{50} of about 5 μM was measured for both of them.

Since some PRDX inhibitors act on the dimeric form of the protein,[14] we also evaluated if the observed modulation of PRDX1 activity by **VIe** and **VIf** related to the presence of oligomers of the protein. For this aim, we performed mass spectrometry analyses of reaction mixtures similar to those used for the inhibition assays; in all the experiments only monomeric PRDX1 was observed.

Structural Basis of PRDX1 Inhibition by FAA Derivatives

PRDX1 is a member of PRDX family, a class of enzymes that catalyze the reduction of hydroperoxides.[15] PRDXs rely on the presence of a cysteine residue that is essential for catalytic activity, the so-called “peroxidatic” cysteine (C52). On the basis of the existence and location of a second cysteine residue, the “resolving” cysteine (C173), the mammalian PRDXs are classified into the following subfamilies: typical 2-Cys PRDXs (PRDX1-PRDX4), atypical two-Cys PRDXs (PRDX5) and one-Cys PRDXs (PRDX6). In the case of PRDX1, the sulfur atom of C52 has been reported to be the active center for peroxidation. During catalysis, the sulfhydryl group of C52 is firstly oxidized to sulfenic acid by hydroperoxides, and then the sulfenic acid is further oxidized to form an intermolecular disulfide bond with the “resolving” cysteine from the other subunit of the dimer. Then, the disulfide bond can be reduced by disulfide reductases, such as thioredoxin, restoring the enzyme activity, and completing the catalytic cycle.

To provide an explanation at the molecular level for the inhibitory activity of FAAs towards PRDX1, we undertook docking studies of **VIe** into the PRDX1 active site using the Schrödinger Glide algorithm.[16] For this purpose, we selected the dimer X-ray crystal structure of the heme-binding protein 23 kDa (HBP23), a rat isoform of PRDX1 with more than 90% of sequence homology with human PRDX1 (PDB code: 1QQ2).[17] In this structure, the active residue C52 from monomer A formed a disulfide bond with C173 from monomer B by C-terminal tail swapping in the dimer. Since the protein did not dimerize in the presence of the inhibitor, as confirmed by mass spectroscopy experiments, docking experiments were conducted only on the monomer A of PRDX1.

Compound **VIe** was anchored in a cleft shaped by residues L46-C52, R128, L147 and P148 (Figure 3). Specifically, the amide carbonyl oxygen of the terminal phenyl ring picked up a H-bond with the backbone NH of F50, with a distance of 3.2 Å. Furthermore, the aromatic phenyl ring of **VIe** formed an edge-to-face π–π stacking interaction with F48, as well as hydrophobic interactions with L46 and F50. A cation-π interaction was also detected between the *ortho*-methoxy phenyl ring and R128. Several hydrophobic interactions between the cinnamoylpyrrolidine moiety and V51, C52, L147 and P148 side chains additionally stabilized the ligand/PRDX1 complex. Notably, site-directed mutagenesis studies showed that F50 and R128 residues play a critical role for PRDX1 catalytic activity toward H_2O_2 and also have an influence on inhibitor binding.[18]

This article is protected by copyright. All rights reserved.

Accepted Manuscript

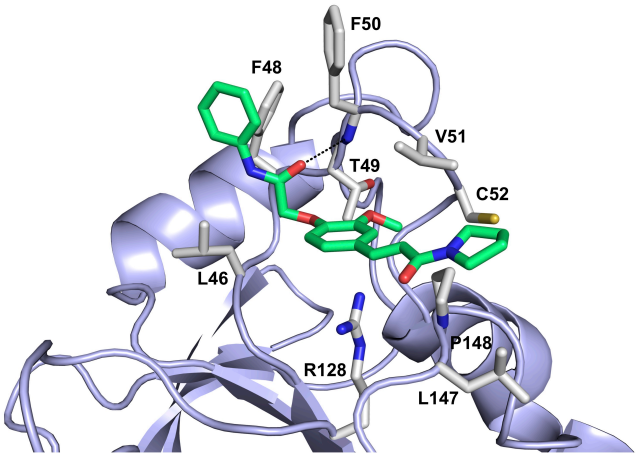

Figure 3. Binding mode of compound **VIe** (green sticks) into PRDX1 active site (PDB code: 1QQ2) represented as a light blue ribbon model. Only the main protein residues are displayed (white sticks) and labeled. The H-bond discussed in the text is depicted as a dashed black line.

Since in the enzymatic activity assay the reaction of PRDX1 with **VIe** and **VIf** took place before the catalytic reactions with H_2O_2 were initialized, it can be assumed that these compounds could interfere with the oxidation of the catalytic cysteine to sulfenic acid or even disrupt the formation of the C173-C52 disulfide bond and the dimeric conformation of the enzyme. Therefore, the inhibition of PRDX1 by **VIe** and **VIf** is the result of the disruption of the enzyme catalytic cycle leading to reduced peroxidase activity.

Cytotoxicity Assessment of VIe and VIf Against NIH/3T3 and HepG2 Cells

The cytotoxic effects of **VIe** and **VIf** on NIH-3T3 cells were studied by using the XTT assay as reported previously.[19] Rosiglitazone and Pioglitazone were used as positive controls. Both compounds showed cytotoxicity above 100 μM (data not shown). According to cell viability data, only **VIe** showed a significantly lower cytotoxicity in comparison with Rosiglitazone at 100 μM concentration (Figure S4A of Supporting Information). Based on these in vitro results, **VIe** and **VIf** were considered suitable for the assessment of their in vivo efficacy. Drug-induced liver injury is a very common cause of drug withdrawals and also an important reason for the failure in drug development process.[20] Potential hepatotoxicity of **VIe** and **VIf** was determined using the XTT assay in HepG2 cells. According to our results, both compounds had an IC_{50} value greater than 100 μM. When compounds were administered, even at the highest concentration, the cytotoxicity was similar to that of Rosiglitazone and Pioglitazone (Figure S4B of Supporting Information). This result suggests that compounds **VIe** and **VIf** likely do not possess any hepatotoxicity risk at the tested concentrations, thus exhibiting a wide range of therapeutic safety.

In Vitro Pharmacokinetic Properties of VIe and VIf

Pharmacokinetic properties of probe compounds and drug candidates ultimately determine how these compounds behave/perform in preclinical animal models and clinical trials.[21] Lipophilicity is an important factor for the pharmacokinetic behavior of drugs. It strongly influences membrane passive permeability, which is required for oral absorption and access of the drug to intracellular compartments and tissue penetration. A measure of lipophilicity can be deduced from the distribution coefficient (logD) that is generally used to represent the partition of an ionic compound between octanol and PBS buffer. An analysis of 232 drugs for which human PK data was available has shown that the logD range for obtaining a highly bioavailable drug is between 2 and 3.[22] As illustrated in Table S4 of Supporting Information, compounds **VIe** and **VIf** had a logD value of 2.84 and 2.03, respectively, indicating good oral bioavailability.

Using in vitro assays, we also measured the permeability[23] for the two compounds **VIe** and **VIf** in both Caco-2 and MDCK-II models. Apparent permeability coefficients (P_{app}) from A-to-B (apical to basolateral of the cell monolayers) and B-to-A (basolateral to apical of the cell monolayers) were obtained by measuring the amount of the compound transported from the donor compartment at 2 μM to the receiver compartment after 150 min incubation. Quantification was done by LC-MS/MS. P-glycoprotein (P-gp) substrate activity was assessed by the efflux ratio (the ratio of P_{app} in the B-to-A direction over that in the A-to-B direction). Furosemide, carbamazepine, domperidone, digoxin, fenoterol, prazosin and quinidine were used as standards for this study.

As shown in Table S4 of Supporting Information, compound **VIf** exhibited asymmetric transport across both Caco-2 and MDCK-II monolayers ($P_{app,A-B}$ of 22.9 × 10^{-6} cm/sec for Caco-2 and 16.7 × 10^{-6} cm/sec for MDCK-II; $P_{app,B-A}$ of 21.6 × 10^{-6} cm/sec for Caco-2 and 15.4 × 10^{-6} cm/sec for MDCK-II), suggesting that it may be orally absorbed in animal models. A compound with an efflux ratio ($P_{app,B-A}/P_{app,A-B}$) greater than 2 is typically considered a possible P-gp substrate. Compound **VIf** showed an efflux ratio less than 2 in both Caco-2 and MDCK-II cells, indicating it is not a substrate for efflux pumps and therefore has improved potential for oral absorption. In contrast, the efflux ratio of **VIe** was slightly higher than 2 in both Caco-2 and MDCK-II cells, which indicated that it likely retained weak P-gp substrate activity. Compounds **VIe** and **VIf** were further subjected to in vitro metabolic stability assays using mouse, rat and human liver microsomes (Table S5 of Supporting Information). A few standard drugs were included in this study. From the multispecies liver microsome stability study, compound **VIe** exhibited low half-life ($T_{1/2,int}$) and high clearance ($CL_{int,app}$) in mouse, rat and human liver microsomes, indicating that it may have unfavorable issues associated with metabolic stability. In contrast, compound **VIf** showed moderate clearance across the species tested with $T_{1/2,int}$ of 77.7, 13.34 and 102.5 min, respectively. Accordingly, compound **VIf** was found to be metabolically more stable than **VIe**.

In Vivo Pharmacokinetic Study of VIe and VIf

A bioavailability study of **VIe** and **VIf** was carried out in male Sprague-Dawley rats and the pharmacokinetic parameters are presented in Table 1.

This article is protected by copyright. All rights reserved.

Accepted Manuscript

Table 1. Mean Pharmacokinetic Parameters Following a Single Intravenous (IV) Bolus and Oral (PO) Administration of **VIe** and **VIf** in Male Sprague-Dawley Rats.

Parameters	VIe		VIf	
Route of administration	IV (1 mg/kg)	PO (5 mg/kg)	IV (1 mg/kg	PO (5 mg/kg)
Dose Volume (mL/kg)	5	10	5	10
C_{max} (ng/mL)	50	1.77	226	6.1
T_{max} (h)	0.083	0.5	0.083	0.25
AUC_{last} (h*ng/mL)	14.8	1.04	75.9	15
$T_{1/2}$ (h)	0.244	-	0.153	4.19
MRT_{last} (h)	0.126	0.681	0.194	2.11
T_{last} (h)	0.833	1	1	5.33
C_{last} (ng/mL)	1.88	1.5	3.8	1.64
Vss (L/kg)	1540	-	3.95	-
Cl (mL/min/kg)	15.5	-	304	-
DNAUC (h*ng/mL)/(mg/kg)	14.8	0.208	76	3.0
%F (%BA)	-	1.4	-	4.0

C_{max}: maximum plasma concentration; T_{max}: time to reach the maximum plasma concentration; AUC_{last}: area under the curve from time zero to the last measurable concentration; $T_{1/2}$: plasma elimination half-life; MRT_{last}: Mean Residence Time to the last concentration; T_{last}: Time of last measurable concentration; C_{last}: last observed (quantifiable) plasma concentration; Vss: volume of distribution at steady state; Cl: plasma clearance; DNAUC: oral dose-normalized AUC; F: oral bioavailability.

Following a single intravenous (IV) administration of **VIe** formulation at 1 mg/kg, the mean plasma clearance (Cl) was found to be moderate, 15.5 mL/min/kg, which is approximately 35% of the normal hepatic blood flow of rats (55 mL/min/kg)[24]. The volume of distribution (Vss) was found to be 1540 L/kg, which was very high compared to total body water of 0.7 L/kg in rats indicating large amount of drug distribution to tissues. The terminal plasma elimination half-life ($T_{1/2}$) was found to be short (0.244 h). After a single oral (PO) gavage administration of **VIe** formulation at 5 mg/kg, the median time to reach the maximum plasma concentration (T_{max}) was found to be 0.5 h indicating rapid rate of absorption. The exposure (C_{max} & AUC_{last}) was found to be 1.77 ng/mL and 1.04 h*ng/mL. The absolute oral bioavailability was found to be 1.4 %.

As regards **VIf**, following a single IV administration at 1 mg/kg, the mean plasma clearance was found to be very high, 304 mL/min/kg, which is approximately 5.5-fold of the normal hepatic blood flow of rats (55 mL/min/kg). The volume of distribution was found to be 3.95 L/kg, which was more than 5.5-folds higher than total body water of 0.7 L/kg in rats indicating high distribution to tissues. The terminal plasma elimination half-life was found to be 0.153 h. Finally, a median time of 0.25 h was found for reaching the maximum plasma concentration of **VIf** following a single PO administration at 5 mg/kg indicating rapid rate of absorption. The exposure (C_{max} & AUC_{last}) was found to be 6.1 ng/mL and 15 h*ng/mL. The absolute oral bioavailability was found to be 4%.

Antidiabetic Activity of VIe and VIf on STZ-NA-Induced Type 2 Diabetic Rats

Compounds **VIe** and **VIf** were investigated for their hypoglycemic activity in a STZ-NA-induced diabetic rat model. The test dose was fixed based on the predicted LD_{50} value.[25] A dose lower than 1/20th of predicted LD_{50} value was used for the study. Diabetic rats were orally treated with the test compounds at a dose of 36 mg/kg body weight for a period of 15 days. Fasting blood glucose of control, diabetic-untreated and diabetic-treated rats was tested on Day 1, 3, 7 and 15 of the administration period (Figure 4A and Table 2). Data were statistically analyzed by one-way ANOVA followed by Dunnett's t-test.

Diabetic control animals showed severe hyperglycemia compared to normal animals. The mean blood glucose level in the diabetic control group on Day 1 was 312.53 ± 7.33 mg/dl on Day 1 and 382.33 ± 10.97 mg/dl on Day 15. The standard drug Pioglitazone significantly lowered the blood glucose level to an almost normal value, whereas the test compounds significantly decreased the blood serum glucose level in the diabetic rats on 7th and 15th days, as compared to the diabetic control group. In particular, the data for 15th Day showed that the activity of compound **VIe** was equivalent to Pioglitazone used in the study. This effect could be ascribable to reversal of insulin resistance or increasing insulin secretion possibly by regeneration of damaged pancreatic β-cells.

Table 2. Effect of **VIe** and **VIf** on Fasting Blood Glucose Levels (mg/dl) in STZ-NA Induced Diabetic Rats.

Treatment	**Blood glucose level (mg/dl)**			
Groups	**Day 1**	**Day 3**	**Day 7**	**Day 15**
Normal	74.0 ± 1.35	78.16 ± 2.18	77.5 ± 3.67	79.75 ±5 .48
Diabetic control	312.53 ± 7.33	333.0 ± 9.02	356.0 ± 11.49	382.33 ± 10.97
VIe	358.0 ± 8.70	301.33 ± 4.78*	228.66 ± 4.5**	172.03 ± 2.36**
VIf	372.16 ± 3.85	314.41 ± 14.27*	255.16 ± 4.47	186.34 ± 2.68***
Pioglitazone	342.56 ± 11.26*	246.50 ± 10.92**	156.90 ± 5.39***	126.5 ± 4.91***

*** indicates $p < 0.001$ *vs* diabetic control; **indicates $p < 0.01$ *vs* diabetic control; * indicates $p < 0.05$.

Total hemoglobin (Hb), glycosylated hemoglobin (HbA1c), total cholesterol (TC), triglyceride (TG), high-density lipoprotein cholesterol (HDL-C), low-density lipoprotein cholesterol (LDL-C) and very low-density lipoprotein cholesterol (VLDL-C), urea, creatinine and uric acid levels were also measured by collecting the blood before sacrificing the animals. Diabetic animals showed significant decrease in Hb levels when compared with control animals. Compounds **VIe**, **VIf** and Pioglitazone brought

This article is protected by copyright. All rights reserved.

Accepted Manuscript

back the Hb levels to normal (Figure 4B and Table 3). In addition, HbA1c levels were augmented in diabetic animals as compared with normal control rats. However, oral administration of **VIe**, **VIf** and Pioglitazone to diabetic rats significantly reduced ($p < 0.001$) the levels of HbA1c as compared with those observed in diabetic control rats (Figure 4C and Table 3), thus highlighting their potential to prevent the diabetic-associated complications.

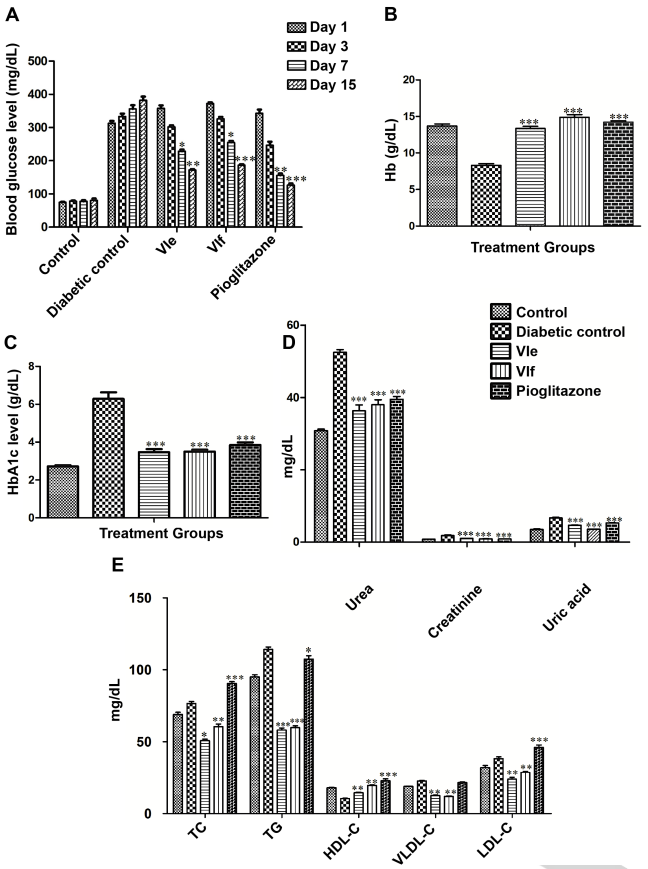

Figure 4. In vivo antidiabetic activity of **VIe** and **VIf** in STZ-NA induced diabetic rats. Effects on the blood glucose levels (A), Hb (B), HbA1c (C), serum urea, creatinine, and uric acid (D), and TC, TG, HDL-C, VLDL-C and LDL-C (E). Data were analyzed by one way ANOVA followed by Dunnett's 't' test and expressed as mean ± SEM from six observations; *** indicates $p < 0.001$ *vs* diabetic control; **indicates $p < 0.01$ *vs* diabetic control; * indicates $p < 0.05$.

Table 3. Effect of Compounds **VIe** and **VIf** on Various Biochemical Parameters in STZ-NA Induced Diabetic Rats.

Groups	Hb	HbA1c	Urea	Creatinine	Uric acid
Normal control	13.7±0.27	2.71±0.06	30.83±0.4	0.78±0.02	3.2±0.09
Diabetic control	8.28±0.25	6.28±0.14	52.5±0.78	1.80±0.06	6.6±0.14
VIe	13.31±0.22***	2.93±0.13***	36.5±1.60***	0.98±0.02***	4.6±0.08**
VIf	14.01±0.26***	3.35±0.14***	38.0±1.36***	0.88±0.03***	3.6±0.23**
Pioglitazone	14.2±0.19***	3.76±0.13***	41±0.76**	0.84±0.017***	3.41±0.36***

*** indicates $p < 0.001$ *vs* diabetic control; **indicates $p < 0.01$ *vs* diabetic control.

Renal markers, such as the plasma levels of urea, uric acid and creatinine were also measured, as diabetes mellitus also causes renal damage due to elevated glucose and glycosylated protein tissue levels, haemodynamic changes within the kidney tissue,[26] and increased oxidative stress,[27] **VIe**-, **VIf**- and Pioglitazone-treated groups showed a declined level of renal markers similar to normal rats, thus revealing their beneficial effect in renal dysfunction (Figure 4D and Table 3).

Figure 4E shows the level of plasma lipid profile such as TG, TC, HDL-C, LDL-C, and VLDL-C. It was observed that diabetes induced an increase in the total cholesterol levels as well as triglyceride levels. Plasma TG, TC, LDL-C, and VLDL-C levels were significantly elevated and HDL levels were reduced in diabetic rats when compared with control rats. Oral treatment with **VIe**, **VIf** and Pioglitazone normalized the diabetes-induced hyperlipidemia, showing significant reduction in TC, TG, LDL-C and VLDL-C levels and an increase in HDL-C levels as compared with diabetic control group (Table 4).

Table 4. Effect of **VIe** and **VIf** on Lipid Profile in STZ-NA-Induced Diabetic Rats.

Groups	TC	TG	HDL-C (mg/dl)	VLDL-C (mg/dl)	LDL-C (mg/dl)
Normal control	95.05±1.43	69.01±1.52	18.01±0.25	18.9±0.24	32.1±1.50
Diabetic control	114.5±1.64	76.5±1.45	10.5±0.0.22	22.7±0.30	38.4±1.18
VIe	50.33 ±1.40**	59.8±1.40**	14.16±0.40**	12.4±0.28*	24.16±1.24**
VIf	60.1±2.88*	59.5±1.30**	19.8±0.30**	11.96±0.26*	22.13±2.70**
Pioglitazone	107.33±2.45*	90.5±1.23***	22.83±1.30***	21.44±0.49***	46.13±1.85**

*** indicates $p < 0.001$ *vs* diabetic control; **indicates $p < 0.01$ *vs* diabetic control; * indicates $p < 0.05$.

Histopathological studies of pancreas and liver

Histopathological observations of pancreas and liver were carried out at 40x magnifications using haematoxylin and eosin (HE) staining. The effects of **VIe**, **VIf** and Pioglitazone on pancreatic and liver tissues are shown in Figures 5 and 6, respectively. Microscopic examinations of the pancreas sections showed the normal histology of the pancreas in normal non-diabetic rats of control group (Figure 5A). By contrast, a severe deterioration emerged in the STZ-NA-induced diabetic rats, including hypochromatosis, lymphocyte infiltration and loss of cell borders in the pancreatic islets (Figure 5B). After treatment with **VIe**, **VIf** and Pioglitazone at 36 mg/kg body weight, improvement in the pancreatic tissues could be observed, which was proved by diminished infiltration and more cohesive cell

This article is protected by copyright. All rights reserved.

Accepted Manuscript

structure in the pancreatic islets in comparison with the diabetic control group animals (Figures 5C-E).

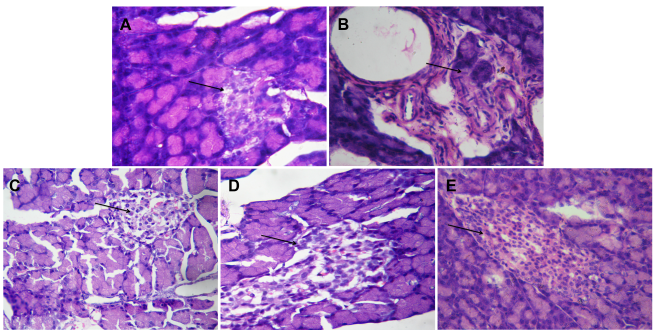

Figure 5. Histopathological analysis of pancreas in normal and STZ-NA-induced diabetic Wistar rats. (A) Normal Control; islets with normal cellular characteristics. (B) Diabetic control; significant reduction in islet volume and number. (C) STZ-NA-induced diabetic rats treated with compound **VIe** (36 mg/kg body weight). (D) STZ-NA-induced diabetic rats treated with compound **VIf** (36 mg/kg body weight). (E) STZ-NA-induced diabetic rats treated with Pioglitazone (36 mg/kg body weight). In diabetic control rats degenerative and necrotic changes with shrunken islets of Langerhans were clearly observed. An improvement in the volume of islets was noted after treatments with Pioglitazone and compounds **VIe** and **VIf**. Examinations were carried out at 40x magnifications with hematoxylin-eosin's staining.

These results indicated that treatment with FAA derivatives could repair islet injury and recuperate the structural integrity of pancreatic islet β-cells and tissues. Histopathological assessment of the normal liver tissue of the non-diabetic rats confirmed the normal structure of the mammalian liver. Each lobule consisted of interconnecting plates of epithelial cells called hepatocytes, which were radially arranged around a central vein (Figure 6A). In contrast, liver sections of STZ-NA-induced diabetic rats disclosed hepatocellular damage consisting in the liver architectural distorsion, fibrosis, inflammation and leucocyte infiltration around the central vein (Figure 6B). Sections of the liver in diabetic rats treated with compounds **VIe**, **VIf** and Pioglitazone showed a morphology similar to that of the healthy group (Figures 6C-E).

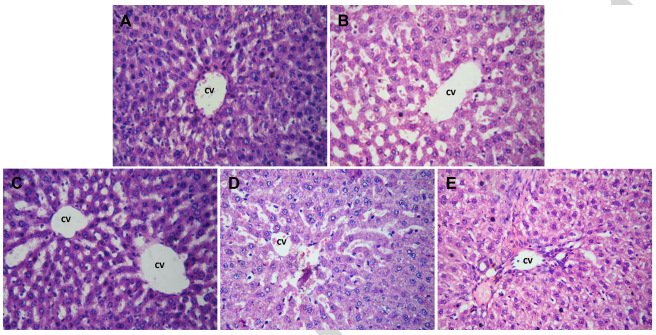

Figure 6. Histopathological analysis of liver in normal and STZ-NA-induced diabetic Wistar rats. (A) Normal control. (B) Diabetic control. (C) STZ-NA-induced diabetic rats treated with compound **VIe** (36 mg/kg body weight). (D) STZ-NA-induced diabetic rats treated with compound **VIf** (36 mg/kg body weight). (E) STZ-NA-induced diabetic rats treated with Pioglitazone (36 mg/kg body weight). The normal rats group demonstrated normal architecture with a central vein and hepatocytes surrounding this vein, while the diabetic control exhibited more sinusoidal space. Groups treated with Pioglitazone and compounds **VIe** and **VIf** showed a morphology similar to that of the healthy group. Examinations were carried out at 40x magnifications with hematoxylin-eosin's staining.

Conclusion

In this study, we designed and synthesized a series of new FAA derivatives resulting from thiazolidinedione ring opening and introduction of a double bond at position C5-C6 of the classical PPARγ agonists TZDs (compounds **VIa-m** in Figure 1). Ferulic acid and its FAA derivatives were previously reported to stimulate insulin secretion in rat pancreatic RIN-5F cells, showing antidiabetic potential.[7] Moreover, ferulic acid possesses antioxidant activity and exerts hypoglycemic effect in STZ-induced diabetic mice and KKAy mice, as well as synergistic interaction with commercially available antidiabetics in STZ-induced diabetic rats.[8] A PPAR-driven luciferase reporter gene assay showed that **VIa-m** failed to offer a significant activation of any of the three PPAR subtypes, even though SPR showed that eleven out of thirteen derivatives had a specific, although weak, binding affinity towards PPARγ. We can speculate that the chemical modifications introduced in FAAs caused the loss of the structural determinants necessary to interact with the residues crucial for receptor activation. Therefore, in order to assess whether FAAs might engage molecular targets other than PPARs, we resorted to a chemical proteomics approach. First, DARTS experiments identified four putative targets for compounds **VIe** and **VIf**. Second, SPR analyses confirmed the direct interaction between PRDX1 and both compounds, indicating their non-covalent bonding. Third, **VIe** and **VIf** inhibited PRDX1 activity in a concentration-dependent manner with IC_{50} of ≅ 5 μM. Last, docking experiments shed light, at the molecular level, on the ability of these two compounds to interfere with the enzyme catalytic cycle. Furthermore, compounds **VIe** and **VIf** had sufficient pharmacokinetics to support in vivo studies and demonstrated no negative effects on metabolic parameters in 15-days treated rats. These compounds significantly decreased blood glucose levels in diabetic rats, lowered urea, uric acid and creatinine levels compared to diabetic control rats, indicating their reno-protective role in preventing diabetic nephropathy. Moreover, they reduced TC, TG, LDL-C, and VLDL-C level to a significant extent, and increased the beneficial HDL-C level suggesting improved insulin sensitivity in the adipose tissue of the treated rats. This action could be beneficial in preventing diabetic complications like coronary heart diseases and atherosclerosis in diabetic condition. Finally, histopathological examination demonstrated that treatment with these two FAAs promoted regeneration of pancreas and liver tissues.

PRDX1 is a member of the PRDX family of cysteine-dependent peroxidase enzymes, which play a dominant role in regulating peroxide levels in the cells.[28] PRDX1 is a multifunctional protein that acts as a hydrogen peroxide scavenger, molecular chaperone, and immune modulator. It is noteworthy that the function of PRDX1 is not restricted to its antioxidant activity; novel roles of PRDX1 have been recognized in cancers, cardiovascular diseases, diabetes and neurodegeneration.[18, 29] Intriguingly, a recent report suggested that the plasma levels of PRDX1 and other PRDX members were higher in T2DM than in control subjects suggesting a potential involvement of PRDX proteins in the development of diabetes mellitus. This pathology is the result of many pathological factors, such as inflammation and intracellular stress. Given that PRDX1 increases the expression of pro-inflammatory cytokines, its participation in the regulation of chronic inflammation and the resultant insulin

This article is protected by copyright. All rights reserved.

Accepted Manuscript

resistance might be speculated.[30] The molecular mechanism by which PRDX1 is involved in insulin signaling and T2DM has been recently investigated showing that the overexpression of this enzyme could induce hepatic insulin resistance by activating p38 mitogen-activated protein kinase (p38MAPK). By contrast, inhibition of p38MAPK activity significantly reversed PRDX1-induced attenuation of insulin signaling suggesting that PRDX1 could be an important signaling transmitter implicated in insulin resistance and onset of diabetes.[11] Therefore, it is reasonable to hypothesize that **VIe** and **VIf** induce their metabolic effects by acting as PRDX1 inhibitors. As reported above, in the STZ-NA-induced diabetic rats, these compounds preserve the normal histological appearance of liver and recuperate the structural integrity of pancreatic islet β-cells and tissues. However, while writing this paper, Stancill and coll. reported that PRDX1 represents a primary defense mechanism against oxidative stress and either pharmacological PRDX1 inhibition with conoidin A or its specific depletion sensitize INS 832/13 cells and rat islets to DNA damage and death induced by hydrogen peroxide or peroxynitrite.[31] This result seems in disagreement with our assumption, however, two aspects should be taken into account: the experimental models and the characteristics of the inhibitors. Firstly, differently from what reported in the literature, we used an in vivo model, which means that inhibition effects on PRDX1 could be counterbalanced by anti-oxidative enzymes like catalase, glutathione peroxidase and others. Secondly, in the Stancill's paper, a covalent inhibitor (conoidin A) was used that binds to the peroxidatic cysteine of PRDX1 preventing irreversibly its antioxidant activity; our molecules, instead, behave as non-covalent inhibitors, as demonstrated by SPR analysis, so they would be able to reduce but not completely abolish PRDX1 activity.

To the best of our knowledge, **VIe** and **VIf** are the first examples of PRDX1 inhibitors able to ameliorate hyperglicemia and hyperlipidemia in a diabetic rat model. Even though further studies are needed to definitely clarify the precise role of PRDX1 in the regulation of insulin resistance and diabetes, these results suggest that this enzyme could represent a new therapeutic target for the treatment of these pathologies.

Experimental Section

Chemistry

Chemicals and solvents were of reagent grade and purchased from Sigma Aldrich/Merck/Spectro-chem/CDH. All reactions were conducted in oven-dried glassware under nitrogen atmosphere, unless otherwise specified. The progress of reactions was monitored on pre-coated TLC plates (silica gel 60 F-254, Merck™, KGaA, Germany). Melting points were determined on an OPTIMELT automated system apparatus and were uncorrected. Compounds were purified by recrystallization using suitable solvents. Final compounds were characterized by their ^{1}H NMR (300 MHz, ECX-500, JEOL and 400 MHz, VNMRS400), ^{13}C NMR (400 MHz, VNMRS400), in either $CDCl_3$ or DMSO-d_6 as a solvent. The purity of all tested compounds was >95%, as confirmed by combustion analysis carried out with a Eurovector Euro EA 3000 model analyzer (Table S6). Mass spectra were recorded by WATERS-Q-T of Premier-HAB213 using the electrospray ionization-mass spectrometry (ESI-MS) technique. Synthesis of ferulic acid was done by the procedures reported by Xia *et al*.[32] Conversion of **I** to **II** was done by the procedure reported earlier.[33] Intermediates **III**, **IVa-m** and **Va-Vm** were prepared by using the procedures reported earlier.[34,35]

General procedure for the preparation of the FAA derivatives (VIa-m)

To the stirred solution of **Va-m** in dimethylformamide were added potassium carbonate and 2-chloroacetamide derivatives. The solution was stirred for 72-80 h. After completion of the reaction, the reaction mixture was then poured into ice-cold water and extracted with dichloromethane. The organic layer was dried with anhydrous Na_2SO_4 and evaporated in vacuo. The crude product thus obtained was purified by recrystallization from CH_2Cl_2/MeOH to afford final compounds.

3-(3-Methoxy-4-(2-oxo-2-(phenylamino)ethoxy)phenyl)-N-phenylacrylamide (VIa): White amorphous powder, yield: 65%, mp 222-224 °C. ^{1}H NMR (400MHz, DMSO-d_6) δ: 10.13 (d, *J*=16 Hz, 1H), 8.32 (s, 1H), 7.70 (d, *J*=8.0 Hz, 1H), 7.63 (d, *J*=8.0 Hz, 1H), 7.54 (d, *J*=16 Hz, 1H), 7.35-7.28 (m, 6H), 7.18 (d, J=8.0 Hz, 1H), 7.11-7.04 (m, 3H), 7.01 (d, J=8.0 Hz, 1H), 6.73 (d, *J*=16 Hz, 1H), 4.76 (s, 2H), 3.89 (s, 3H). ^{13}C NMR (100MHz, DMSO-d_6) δ: 166.7, 164.2, 149.6, 149.4, 140.5, 139.8, 138.8, 129.2, 129.0, 124.1, 121.9, 119.9, 119.6, 114.2, 111.0, 68.5, 56.0. ESI MS (m/z): $(M+1)^+$ calcd. for $C_{24}H_{22}N_2O_4$, 402.45; found, 403.00.

N-Benzyl-3-(3-methoxy-4-(2-oxo-2-(phenylamino)ethoxy)phenyl)acrylamide (VIb): White crystalline solid, yield: 68%, mp 160-162 °C. ^{1}H NMR (400MHz, DMSO-d_6) δ: 10.05 (s,1H); 8.49 (t, *J*=6 Hz, 1H), 7.60 (s, 1H), 7.58 (s, 1H), 7.04-7.60 (m, 11H), 6.95 (d, *J*=8.4 Hz, 1H), 6.58 (d, *J*=16 Hz, 1H), 4.71 (s, 2H), 4.37 (d, *J*=5.6 Hz, 2H), 3.83 (s, 3H). ESI MS (m/z): $(M+1)^+$ calcd. for $C_{25}H_{24}N_2O_4$, 417.47; found, 417.20.

3-(3-methoxy-4-(2-oxo-2-(phenylamino)ethoxy)phenyl)N-phenethylacrylamide (VIc): White crystalline solid, yield: 65% mp 165-167 °C. ^{1}H NMR (400MHz, DMSO-d_6) δ: 10.07 (s, 1H), 8.09 (s, 1H), 7.58-7.3 (m, 13H), 7.05 (d, *J*=8 Hz, 1H), 6.92 (d, *J*=12 Hz, 1H), 4.69 (s, 2H), 3.81 (s, 3H), 3.37 (t, *J*=12 Hz & *J*=8 Hz, 2H), 2.73 (t, *J*=6 Hz, 2H). ^{13}C NMR (100 MHz, DMSO-d_6) δ: 166.8, 149.6, 139.9, 138.8, 138.8, 129.2, 129.0,128.8, 126.5, 121.5, 120.8, 119.8, 114.3, 111.0, 56.0, 40.7, 35.6. ESI MS (m/z): $(M+1)^+$ calcd. for $C_{26}H_{26}N_2O_4$, 430.47; found, 431.00.

N-Cyclohexyl-3-(3-methoxy-4-(2-oxo-2-(phenylamino)ethoxy)phenyl)acrylamide (VId): White amorphous powder, yield: 78% mp 165-167 °C. ^{1}H NMR (400MHz, DMSO-d_6) δ: 10.09 (s, 1H), 8.31 (s, 1H), 6.50-8.31 (m, 10H), 4.73 (s, 2H), 3.85 (s, 3H), 1.16-1.67 (m, 11H). ^{13}C NMR (100MHz, DMSO-d_6) δ: 166.8, 164.5, 149.6, 148.9, 138.8, 138.6, 129.4, 129.2, 124.1, 121.4, 119.8, 114.3, 110.8, 68.5, 55.9, 47.9, 32.9, 25.7, 25.0. ESI MS (m/z): $(M-1)^+$ calcd. for $C_{24}H_{28}N_2O_4$, 408.49; found, 409.10.

2-(2-Methoxy-4-(3-oxo-3-(pyrrolidin-1-yl)prop-1-enyl)phenoxy)-N-phenylacetamide (VIe): White crystalline solid, yield: 47% mp 202-204°C. ^{1}H NMR (400MHz, $CDCl_3$) δ: 8.97 (s, 1H), 6.94 7.61 (m, 9H), 6.62 (d, *J*= 16.0 Hz, 1H), 4.65 (s, 2H), 3.97 (s, 3H), 1.61 1.98 (m, 8H). ^{13}C NMR (100MHz, DMSO-d_6) δ: 166.8,164.1, 149.6, 149.1, 140.6, 138.8, 129.4, 129.2, 124.1, 122.1, 119.8, 118.5, 114.1, 111.5, 68.5, 56.2, 46.5, 46.0, 26.0, 24.0. ESI MS (m/z): $(M+1)^+$ calcd. for $C_{22}H_{24}N_2O_4$, 380.14; found, 381.10.

2-(2-Methoxy-4-(3-morpholino-oxoprop-1-enyl)phenoxy)-N-phenylacetamide (VIf)*:* White crystalline solid, yield: 62% mp 212-214 °C. ^{1}H NMR (400MHz, $CDCl_3$) δ: 8.89 (s, 1H), 7.13-7.59 (m, 8H), 6.98 (d, *J*=8 Hz, 1H), 6.46 (d, *J*= 16Hz, , 1H), 4.67 (s, 2H), 3.99 (s, 3H), 0.86-1.60 (m, 8H).^{13}C NMR (100MHz, DMSO-d_6) δ: 168.8, 166.2, 165.8, 151.6, 145.1, 141.5, 138.9, 133.4, 129.2, 124.1, 123.9, 123.7, 122.1, 119.8, 119.6, 118.2, 112.4, 63.1, 56.4, 56.1, 20.8. ESI MS (m/z): $(M+1)^+$ calcd. for $C_{22}H_{24}N_2O_5$, 397.17; found, 397.10.

This article is protected by copyright. All rights reserved.

Accepted Manuscript

2-(2-Methoxy-4-(3-oxo-3-(piperidine-1-yl)-prop-1-en-1-yl)phenoxy)-N-phenylacetamide **(VIg)**: White crystalline solid, yield: 60% mp 192-194 °C. ^{1}H NMR (400MHz, DMSO-d_6) δ: 10.17 (s, 1H), 6.82-7.76 (m, 10H), 4.81 (s, 2H), 3.85 (s, 3H), 2.52 (q, 8H), 2.28 (s, 2H). ESI MS (m/z): $(M+1)^+$ calcd. for $C_{23}H_{26}N_2O_4$, 394.19; found, 395.10.

3-(3-Methoxy-4-(2-oxo-2-(phenylamino)ethoxy)phenyl)-N-methylacrylamide (VIh): White crystalline solid, yield: 78% mp 220-222 °C. ^{1}H NMR (400MHz, DMSO-d_6) δ: 10.10 (d, 1H), 6.66-7.74 (m, 11H), 4.77 (t, *J*=8.8 Hz, 2H), 3.85 (d, *J*=14 Hz, 3H), 2.26 (s, 3H). ESI MS (m/z): $(M+2)^+$ calcd. for $C_{19}H_{20}N_2O_4$, 340.14; found, 342.0.

N-Ethyl-3-(3-methoxy-4-(2-oxo-2-(phenylamino)ethoxy)phenyl)acrylamide (VIi): White crystalline solid, yield: 56% mp 269-271 °C. ^{1}H NMR (400MHz, DMSO-d_6) δ: 10.10 (s, 1H), 8.05 (s, 1H), 6.47-7.60 (m, 10H), 4.72 (s, 2H), 3.84 (s, 3H), 3.18 (t, *J*=5.96 Hz, 2H), 1.05 (t, *J*=7.2 Hz, 3H). ESI MS (m/z): $(M-1)^+$ calcd. for $C_{20}H_{22}N_2O_4$, 354.14; found, 355.10.

N-Butyl-3-(3-methoxy-4-(2-oxo-2-(phenylamino)ethoxy)phenyl)acrylamide (VIj*:* White crystalline solid, yield: 64% mp 134-136 °C. ^{1}H NMR (400MHz, DMSO-d_6) δ: 10.10 (s, 1H), 8.05 (s, 1H), 6.47-7.60 (m, 10H), 4.72 (s, 2H), 3.86 (s, 3H), 3.67-3.84 (m, 2H), 3.38-3.47 (m, 2H), 3.17 (t, *J*=6.96 Hz, 2H), 1.05 (t, *J*=7.2 Hz, 3H), ESI MS (m/z): M^+ calcd. for $C_{22}H_{26}N_2O_4$, 382.12; found, 382.93.

N-Isopropyl-3-(3-methoxy-4-(2-oxo-2-(phenylamino)ethoxy)phenyl)acrylamide (VIk): White crystalline solid, yield: 60% mp 162-164°C. ^{1}H NMR (400MHz, DMSO-d_6) δ: 8.80 (s,1H), 5.76-7.58 (m, 11H), 4.62 (s, 2H), 4.20 (sex, *J*=19.6, 6 Hz, 1H), 3.96 (s, 3H), 1.21 (d, 6H). ^{13}C NMR (100MHz, $CDCl_3$) δ: 166.5,165.1, 149.8, 148.3, 140.2, 137.1, 130.4, 129.1, 124.8, 121.4, 120.2, 120.0, 115.9, 110.9, 69.9, 56.0, 41.8, 22.9. ESI MS (m/z): $(M+1)^+$ calcd. for $C_{21}H_{24}N_2O_4$, 368.14; found , 369.1.

3-(3-Methoxy-4-(2-oxo-2-(phenylamino)ethoxy)phenyl)-N,N-dimethylacrylamide (VIl): White crystalline solid, yield: 55% mp 145-147 °C. ^{1}H NMR (400MHz, DMSO-d_6) δ: 10.10 (s, 1H), 8.03 (s, 1H), 6.48-8.03 (m, 9H), 4.71 (s, 2H), 3.84 (s, 3H), 3.15 (t, *J*=6.8 Hz, 3H), 0.87 (t, *J*=7.24 Hz, 3H). ESI MS (m/z): $(M+1)^+$ calcd. for $C_{20}H_{22}N_2O_4$, 354.14; found, 355.10.

N,N-Diethyl-3-(3-methoxy-4-(2-oxo-2-(phenylamino)ethoxy)phenyl)acrylamide (VIm): White crystalline solid, yield: 61% mp 175-177 °C. ^{1}H NMR (400MHz, $CDCl_3$) δ: 8.80 (d, 1H), 6.99-7.66 (m, 9H), 6.72 (d, *J*=16 Hz, 1H), 4.64 (s, 2H), 3.97 (s, 3H), 3.47-3.92 (m, 4H), 1.19-1.28 (m, 6H). ESI-MS (m/z): $(M+1)^+$ calcd. for $C_{22}H_{26}N_2O_4$, 381.14; found, 383.10.

Transactivation Assay

Reference compounds, the medium, and other cell culture reagents were purchased from Sigma-Aldrich (Milan, Italy).

Plasmids

The expression vectors expressing the chimeric receptor containing the yeast Gal4-DNA binding domain fused to either the human PPARα, PPARγ or PPARδ LBD and the reporter plasmid for these Gal4 chimeric receptors (pGal5TKpGL3) containing five repeats of the Gal4 response elements upstream of a minimal thymidine kinase promoter that is adjacent to the luciferase gene were described previously.[36]

Cell culture and Transfections

Human hepatoblastoma cell line HepG2 (Interlab Cell Line Collection, Genoa, Italy) was cultured in minimum essential medium (MEM) containing 10% of heat-inactivated foetal bovine serum, 100 U of penicillin G/mL, and 100 µg of streptomycin sulfate/mL at 37 °C in a humidified atmosphere of 5% CO_2. For transactivation assays, 10^5 cells per well were seeded in a 24-well plate and transfections were performed after 24 h with CAPHOS, a calcium phosphate method, according to the manufacturer's guidelines. Cells were transfected with expression plasmids encoding the fusion protein Gal4-PPARα-LBD, Gal4-PPARγ-LBD, or Gal4-PPARδ-LBD (30 ng), pGal5TKpGL3 (100 ng), and pCMVβgal (250 ng). Four hours after transfection, cells were treated for 20 h with the indicated ligands and reference compounds in duplicate. All compounds were tested at two concentrations (5 and 25 µM). Luciferase activity in cell extracts was determined by a luminometer (VICTOR^3 V Multilabel Plate Reader, PerkinElmer). β-Galactosidase activity was determined using ortho-nitro-phenyl-β-D-galactopyranoside as described previously.[37] All transfection experiments were repeated at least twice.

DPPH assay

The DPPH radical scavenging assay was performed in 96-well microplates as previously reported.[38] Briefly, a freshly prepared solution of DPPH in methanol (100 µM final concentration) was added to a methanolic solution of test compounds. The mixtures were shaken vigorously and left to stand in the dark for 30 min at room temperature, then absorbance was read at 520 nm using a spectrophotometric plate reader (Victor 3 Perkin-Elmer). The antioxidant activity was determined as the RSA% (radical scavenging activity), calculated using the following equation:

$$RSA\% = 100x[(Ao-Ai)/Ao]$$

where Ao and Ai are the DPPH absorbance in the absence or in the presence of antioxidant, respectively. Different sample concentrations were used in order to obtain antiradical curves for calculating the EC_{50} values. Antiradical curves were plotted referring to concentration on the x axis and their relative scavenging capacity on the y axis. The EC_{50} values and statistical analyses were processed using GraphPad Prism 5.0 software (San Diego, CA). Values of all parameters are expressed as mean ± SEM of three independent measurements in triplicate.

Surface Plasmon Resonance

All SPR experiments were performed on a BIACORE 3000 instrument (GE-Healthcare) according to our previously published procedure.[39] Briefly, PPARα, PPARγ, PPARδ, Hsp90, Hsp70, Annexin 6 and Peroxireodxin 1 were immobilized on a research-grade CM5 sensor chips (GE Healthcare) using a standard amine-coupling protocol. A density of 3-5 kRU (1000 RU corresponds to the binding of ~ 1 ng per square mm of protein on the dextran surface) was achieved. Compounds were injected on each protein chip at four different concentrations ranging from 0.5 to 50 µM. Positive control, Rosiglitazone, was injected at concentrations ranging from 0.1 to 100 nM. Measurements were performed at 25 °C, using a 50 µL min^{-1} flow rate. Association and dissociation times were set at 60 s and 300 s, respectively. Interactions curves were fit to a single-site bimolecular interaction model to yield K_D. BIAevaluation software (GE Healthcare) was used for sensorgrams elaboration.

DARTS Experiments

HepG2 cells were treated with 25 µM **VIe**, **VIf** or DMSO for 2 h. Following the incubation, cells were lysed in PBS containing 0.1% Igepal (lysis buffer) and phosphatase inhibitor cocktail (P8340, Sigma-Aldrich, St. Louis, MO, USA). Protein concentrations were determined by a Bio-Rad DC Protein Assay (Bio-Rad, Hercules, CA, USA) using bovine albumin as standard. All steps were performed on ice or at 4 °C. Samples were warmed to room temperature and digested enzymatically with subtilisin (enzyme:lysate 1:1000 w/w for 30 min at 30 °C). The resulting mixtures

This article is protected by copyright. All rights reserved.

Accepted Manuscript

were separated by SDS-PAGE and stained with Coomassie Blue. Gel lanes showing significant differences in intensity in the different samples were excised manually and subjected to an in-gel digestion procedure. Peptides were analyzed by high-resolution LC-MS/MS, using a Orbitrap XL mass spectrometer (Thermo Fisher Scientific Inc., Rockford, IL USA) equipped with a nanospray ion source and coupled to a nano-Acquity capillary UPLC system (Waters, Milford, MA, USA). Mass spectra were acquired over a 400 to 1800 *m/z* range, and MS/MS spectra over a 25 to 2000 *m/z* range. MS and MS/MS data were used by Mascot (Matrix Science) to interrogate the Swiss Prot nonredundant protein database. Settings were as follows: mass accuracy window for parent ion, 5 ppm; mass accuracy window for fragment ions, 250 millimass units; fixed modification, carbamidomethylation of cysteines; variable modifications, oxidation of methionine. Proteins with more than two peptides and program scores >100 were considered as reliable proteins.

PRDX1 Activity Assay

PRDX1 activity was measured in the presence of different amounts of **VIe** or **VIf** using the 2-Cys PRDX Activity Assay Kit (Redoxica), according to manufacturer's instructions, as previously described.[40] Briefly, HepG2 cells were incubated with different concentration of the two compounds for 1 h, then washed with 1× PBS and sonicated in the activity assay buffer. The total reaction volume of 150 µL contained 50 mmol/L HEPES-NaOH buffer, thioredoxin, thioredoxin reductase, and NADPH. The reaction was initiated by the addition of 2 µL of 10 mM H_2O_2. NADH oxidation was spectrophotometrically monitored for 10 minutes at 340 nm.

Mass Spectrometry Analysis of PRDX1 Oligomerization

To verify a possible induction of PRDX1 dimerization by **VIe** and **VIf**, mass spectrometry analyses were performed on mixtures composed by 1 µM PRDX1, 50 mM HEPES-NaOH (pH 7,4), 1 mM NADPH and different amounts of **VIe** or **VIf** (from 10 µM to 100 µM). Mass spectra were acquired using a ESI- Q-TOF premier instrument (Waters) in positive ion mode and over a *m/z* range from 700 to 1500.

Computational Chemistry

Molecular modeling and graphics manipulations were performed using Maestro 11.3 (Maestro, Schrödinger, LLC, New York, NY, 2019) running on an E4 Computer Engineering E1080 workstation provided with an Intel Xeon processor. Figures were generated using Pymol 2.0 (The PyMOL Molecular Graphics System, Version 2.0 Schrödinger, LLC).

Protein and Ligand Preparation

Because the only available crystal structures of the human PRDX1 are complexed with sulfiredoxin,[41] which is a reductant partner enzyme, we used the crystal structure of the rat HBP23 (PDB code: 1QQ2)[17] for docking studies. Human PRDX1 and rat HBP23 share a sequence identity of more than 90%. The HBP23 dimer structure is made up of two identical monomers, A and B; in each monomer the residue C52 forms a disulfide bond with the conserved C173 from another monomer by C-terminal tail swapping.[17] Since the enzyme was not found to dimerize in the presence of **VIe**, docking experiments were conducted only on the monomer A. The four rat-specific residues S14, I88, I144, and I156 were mutated to human-specific residues N14, V88, V144, and T156. In addition, residue S83, which is a mutation that reduces the tendency to form aggregates, was mutated back to cysteine. The protein setup was carried out using the Protein Preparation Wizard implemented in Maestro. Hydrogen atoms were added to the protein consistent with the neutral physiologic pH. Arginine and lysine side chains were considered as cationic at the guanidine and ammonium groups, and the aspartic and glutamic residues were considered as anionic at the carboxylate groups. The protonation and flip states of the imidazole rings of the histidine residues were adjusted together with the side chain amides of glutamine and asparagine residues in a H-bonding network optimization process. Successively, the protein hydrogens only were minimized using the Impref module of Impact with the OPLS_2005 force field. Initial coordinates of compound **VIe** were constructed by using the Molecular Builder module in Maestro. The structure was energy-minimized using Macromodel 11.7 (MacroModel, Schrödinger, LLC, New York, NY, 2019) using the MMFF force field with the steepest descent (1000 steps) followed by truncated Newton conjugate gradient (500 steps) methods. Partial atomic charges were computed using the OPLS-AA force field.

Docking Simulations

Docking of **VIe** was performed with the Schrödinger Glide algorithm.[16] A docking grid was generated, enclosing a box centered on the catalytic thiolate of C52 with an inner box size of 10 × 10 × 10 Å and an outer box of 30 × 30 × 30 Å. A scaling factor of 0.8 was set for van der Waals radii of receptor atoms. Ligand sampling was allowed to be flexible. Default docking parameters were used, and no constraints were included. The results of calculations were evaluated and ranked based on the Glide SP scoring function. The final receptor-ligand complex for each ligand was chosen interactively by selecting the highest scoring pose that was consistent with the experimentally derived information about the binding mode of the ligand.

PAINS Filtering

All the tested compounds were screened for known classes of pan-assay interference compounds (PAINS)[42] by using Faf-Drugs4.[43] None of the compounds was found as potential PAINS.

Cytotoxicity Assessment

The 2,3-bis(2-methoxy-4-nitro-5-sulfophenyl)-2H-tetrazolium-5-carboxanilide (XTT) assay is based on the mitochondrial succinate dehydrogenase activity, which is only active in cells with an intact metabolism. Residual cell viability was measured by metabolism of the XTT substrate to the colored product formazan. NIH/3T3 mouse embryonic fibroblast (ATCC®CRL-1658™) and HepG2 human hepatocellular liver carcinoma (ATCC® HB-8065™) cell lines were employed to investigate the cytotoxicity of the compounds. Cells were incubated according to the instructions of the supplier at 37 °C in a humidified atmosphere of 95% air and 5% CO_2 and were seeded at $1x10^4$ cells into each well of 96-well plates. After 24 hours of incubation, compounds were added to the wells at the concentration range between 100 µM and 0.316 µM concentrations (100; 31.6; 10; 3.16; 1; 0.316 µM) in quadruplicates. The XTT assay (Xenometrix, Switzerland) was performed according to the manufacturer's instructions, after 24 h incubation with the compounds. The absorbance was determined after 2 h incubation at 480 nm with a reference wavelength of 680 nm using a microplate reader (BioTek, USA). Inhibition % was calculated for each concentration of the compounds according to the formula below and IC_{50} values were estimated by plotting a dose-response curve of the inhibition % versus test compound concentrations. Cell viability % was calculated according to growth control absorbance values.

$$\%\ Inhibition = 100 - \frac{(Corrected\ mean\ OD\ sample)}{Corrected\ mean\ OD\ solvent\ controls} \times 100$$

The stock solutions of the compounds were prepared in DMSO and further dilutions were made with fresh culture medium. The final DMSO concentration was under 0.1%. Rosiglitazone and Pioglitazone were used as positive controls. All data were obtained from 3 independent experiments in quadruplicates.

In Vitro Pharmacokinetic Properties of VIe and VIf

Determination of LogD

This article is protected by copyright. All rights reserved.

Accepted Manuscript

Phosphate buffer solution (PBS, pH 7.4) and *n*-octanol were mixed overnight and then the aqueous and organic phases were separated and used for LogD determination. A 4.5 µL of 10 mM compounds (**VIe** and **VIf**) were transferred to 96-well plate (P1). To which 300 µL of *n*-octanol (pre-saturated with PBS) was added and shaken for 2 min using Thermomixer. Then 300 µL of PBS (pre-saturated with *n*-octanol) was added, sealed using sealing tape and shaken vigorously at 850 rpm for 2 h at 25 °C. The plate was then allowed to stand for 30 min and followed by centrifugation at 2000 rpm for 10 min at 25 °C. A 100 µL of *n*-octanol from assay plate was taken out for further dilution. Also 100 µL of PBS layer was taken out. Further, *n*-octanol phase was diluted by 1000-fold and PBS phase by 20-fold. The dilution was completed by mixing well and amount of **VIe** and **VIf** in both the phases were quantified using LC-MS/MS.

$$LogD = \frac{Compound\ concentration\ in\ Organic\ phase\ x\ Relative\ dilution\ factor}{Compound\ concentration\ in\ Buffer\ phase}$$

Determination of Caco-2 and MDCK-II Permeability

Caco-2 and MDCK-II cells were cultured in DMEM media containing 10% Foetal bovine serum and antibiotics following the routine cell culture procedures. Cells (7500 for Caco-2 and 18000 for MDCK-II cells/well) were plated in 96-well inserts (Corning) and grown for 21 and 6 days, respectively. Apical and basal wells were washed with buffer (HBSS containing 10 mM HEPES, pH7.4). Permeability experiment was conducted at 2 µM test concentration at 37 °C for 2.5 h without shaking under 5% CO_2 and 95% RH. The study was conducted in both directions, Apical to Basal and Basal to Apical. Aliquots from acceptor wells were diluted and quantified using LC-MS/MS along with initial donor samples. Membrane integrity of the cell layer was checked by Lucifer Yellow (LY) rejection study. Wells having less than 1% fluorescence intensity with respect to Lucifer yellow dosing solution were considered acceptable. Apparent Permeability was calculated using the formula given below:

$$P_{app} = \left(\frac{V_a}{Area \times Time}\right)\left(\frac{Conc.\ in\ Acceptor\ sample \times Sample\ dilution\ factor}{Conc.\ of\ initial\ donor}\right)$$

where:

V_a = Volume of acceptor well (in mL) = 0.25

Area = Surface area of the membrane (cm^2)

Time = Time of incubation (sec) = 9000

$$Efflux\ ratio = \frac{[P_{app}]\ B\ to\ A}{[P_{app}]\ A\ to\ B}$$

Metabolic Stability Studies

Metabolic stability was determined using human/rat/mouse liver microsomes. Compounds (1 µM) were mixed with microsomes (0.4 mg protein/ml) and reaction was initiated by addition of NADPH regeneration system (1.3 mM NADP, 3.3 mM Glucose-6-phosphate, 3.3 mM $MgCl_2$ and 0.4 U/mL Glucose-6-phosphate dehydrogenase). Reaction was terminated after 0, 5, 10, 20, 30 and 60 min using three volumes of ice-cold acetonitrile followed by vigorous mixing. Samples were centrifuged, supernatant half diluted with water and quantitated using LC-MS/MS. Half-life ($T_{1/2}$) and Clearance ($CL_{int,app}$) were calculated using the formula given below:

$$T_{1/2}(min) = \frac{0.693}{slope\ of\ the \ln vs\ time\ curve}$$

$$CL_{int,app}(\mu l/min/mg) = \ln 2 \times \frac{1}{T_{\frac{1}{2}(min)}} \times \frac{mL\ incubation}{mg\ microsomal\ protein} \times \frac{1000\ \mu L}{mL}$$

In Vivo Pharmacokinetic Study of VIe and VIf

Chemicals and Reagents

MS grade (≥99.0% pure) ammonium acetate and formic acid were sourced from Sigma Aldrich. HPLC grade acetonitrile (ACN), methanol, isopropyl alcohol and dimethyl sulfoxide solvents were purchased from Merck Germany. Milli-Q® Water used for the preparation of mobile phase, rinsing solvent and seal washes was obtained from the inhouse (Eurofins Advinus limited) Milli-Q® system. Compounds **VIe** ($C_{22}H_{24}N_2O_4$, 380.44) and **VIf** ($C_{22}H_{24}N_2O_5$, 396.44) with more than 99% chromatographic purity, were synthesized and characterized at Birla Institute of Technology, Mesra, Ranchi-835215 (JH) India. The internal standard Sulfaphenazole (SPZ, $C_{15}H_{14}N_4O_2S$, 314.36, purity of 99%) used in the study was procured from Sigma Aldrich. Male Sprague-Dawley rats (220-240 g) were obtained from Vivo Bio Tech Ltd. India. A SCIEX API 4000™ LC/MS/MS triple quadrupole mass spectrometer system equipped with a positive Electrospray ionization (ESI) source and Shimadzu prominence HPLC comprising of binary pumps, column oven and SIL-HTC autosampler was used in the study. Data acquisition, integration and quantification were performed using Analyst® 1.6.3.

Chromatographic and Mass Spectrometric Conditions

Liquid chromatographic separation of **VIe**, **VIf** and internal standard, Sulfaphenazole, was achieved on a reverse phase Thermo Hypersil Phenyl BDS, 50 X 4.6 mm, 2.4 µm column operating at 25 °C. The isocratic mobile phase was a 20:80 (v/v) mixture of 10 mM ammonium acetate solution and acetonitrile containing 0.1% formic acid delivered at a flow rate of 0.6 mL/min. Mass spectrometer was operated in positive electrospray ionization mode with unit mass resolution in a quadrupole analyzer with 300 ms dwell time and the analytes were detected by multiple reaction monitoring (MRM). The compound parameters of analytes and internal standard were optimized along with the MRM transition (*m/z)* to achieve sensitivity. Source parameters were optimized to a curtain gas N_2 flow of 25 psi (CUR), nebulizer N_2 gas of 40 psi (gas 1), ion spray voltage of 5500 V (IS), auxiliary N_2 gas of 50 psi (gas 2) with turbo spray temperature of 400 °C (TEMP) and collision-activated dissociation gas (CAD) of 10 psi. MRM transition (m/z) selected for the analytes were **VIe** 381.2→189.3, **VIf** 397.2→310.2 397.2→189.3, 397.2→106.2 and Sulfaphenazole (Internal standard) 315.2→158.1 (Figures S5-8 of Supporting Information). System suitability test was performed prior to analysis of samples. System suitability test comprised of six replicate injections of extracted ULOQ and an extracted blank and LLOQ sample from rat plasma. The percentage coefficient of variation (CV (%)) for peak area ratio (analyte to internal standard) of six replicate injections was ≤2%, which met the acceptance criteria. The retention time was within ±0.5 min variation in each analytical run. *Sample Preparation*. The simple and easy protein precipitation (crashing) method was adopted for the extraction of selected analytes (**VIe** & **VIf**) and internal standard (Sulphaphenazole) from rat plasma samples. To 50 µL aliquot of calibration standard/quality control/validation/study samples in pre-labeled microcentrifuge tubes (1.5 mL capacity), 250 µL of internal standard (100 ng/mL Sulfaphenazole in acetonitrile) was added. All the samples were vortex mixed for about 10 min in a vortex mixer (Vibramax 100 Heidolph Instruments) followed by centrifugation in a refrigerated centrifuge (Eppendorf 5810R) at 10000 rpm and 4 °C for 15 min. About 10 µL of the supernatant sample was injected into API4000 LC-MS/MS system.

Preparation of Calibration Standards and Quality Control Samples

The stock solutions of the analytes (**VIe** and **VIf**) and internal standard (Sulphaphenazole) were prepared in DMSO at 1 mg/mL concentration. The primary stock solutions were further diluted in DMSO to prepare calibration standard solutions in the concentration range of 20 to 20000 ng/mL using DMSO. These solutions were then spiked in interference-free rat blank plasma to obtain calibration standards in the

This article is protected by copyright. All rights reserved.

Accepted Manuscript

pharmacologically relevant range of 1.12 to 2650 (**VIe**) and 1.07 to 2550 (**VIf)** ng/mL. Similarly, the quality control (QC) samples were prepared using independent stock solutions of analytes to obtain the concentrations of 3.18, 995 and 1990 ng/mL in rat plasma, representing low, medium and high concentration QC samples, respectively. The primary stock solution (1 mg/mL) of the internal standard, Sulfaphenazole, was diluted in acetonitrile to prepare a working solution of 100 ng/mL. The primary and intermediate stock solutions, diluted standard solutions, quality control solutions and internal standard solution were stored at 2-8 °C. The spiked plasma samples (calibration standards and quality controls) were prepared freshly prior to sample analysis.

Rat Bioavailability Study

Rats were acclimatized in the laboratory condition for one week prior to experiments and were maintained under standard environmental conditions with a 12 h light/dark cycle with free access to rodent chow and filtered water. All animal experiments were approved by the Institutional Animal Ethics Committee and were in accordance with the Committee for the Purpose of Control and Supervision of Experiments on Animals (CPCSEA), Ministry of Social Justice and Environment, Government of India. Jugular vein cannulation was performed for 12 (n=3) rats 48 hours prior to conduct of experiment and the patency was checked prior to initiation of study. All compounds were injected as intravenous bolus dose at 1 mg/kg and administered orally at 5 mg/kg. Blood samples (approximately 0.250 mL) were collected from the jugular vein at 0.083 (IV only), 0.25, 0.5, 1, 2, 4, 6, 8 24 and 48 h post dose administration into prelabelled microcentrifuge tubes containing dipotassium ethylenediaminetetraacetic acid (K_2EDTA) anticoagulant at the final concentration of 4 mM. The blood samples, after mixing were centrifuged at 2400 g for 10 min at a set temperature of 4 °C. The collected plasma samples were stored below -60 °C until bioanalysis.

Dose Formulation and Vehicle

Intravenous formulation of **VIe** and **VIf** was prepared at 0.2 mg/mL strength in a mixture of 10:90 (v/v) N-Methyl-2-Pyrrolidinone and phosphate buffered saline pH 7.4. Oral formulation of **VIe** and **VIf** at 0.5 mg/mL strength was prepared with dimethyl sulfoxide 5 % (v/v), Cremophor EL 10 % (v/v), polyethylene glycol 400 35 % (v/v) and 0.1 M citrate buffer pH 3.050 % (v/v). Dose volume for intravenous administration was 5 mL/kg and for the oral administration was 10 mL/kg. All the formulations were freshly prepared on the day of dosing and were continuously stirred before dosing. Body weights of the animals were recorded prior to dosing and the body weights were used to determine the volume of formulation to be administered to each animal.

Pharmacokinetics Data Analysis and Bioavailability Study in Male Sprague-Dawley Rats

Pharmacokinetic parameters were calculated by a non-compartmental analysis tool of the validated Phoenix® WinNonlin® 8.0. The area under the curve-time data (AUC_{last} and $AUC_{infinity}$) was calculated by the linear trapezoidal method and $C_{max,}$ and T_{max} were determined by visual observation. Additionally, pharmacokinetic parameters like C_0, clearance (CL), the volume of distribution (Vss), and half-life ($T_{1/2}$), were estimated. Absolute oral bioavailability (%F) was calculated with dose-normalized exposure against dose-normalized intravenous exposure. The elimination rate constant (K_{el}) was calculated by log-linear regression of concentration data during the elimination phase with a correlation coefficient >0.80. The terminal half-life ($t_{1/2}$) was calculated using the formula $0.693/K_{el}$. All the rats were healthy, and no clinical signs were observed during the study period.

In Vivo Antihyperglycemic and Antidyslipidemic Activity Evaluation

Male Wistar rats weighing about 160-220 g were used for animal studies. Experiments were approved by the institutional animal ethical committee (no. PROV/BIT/PH/IAEC/04/2016) of the Department of Pharmaceutical Sciences and Technology, Birla Institute of Technology, Mesra, Ranchi, and were conducted in accordance with National Institutes of Health Guide for Care and Use of Laboratory animals. Animals were housed in polypropylene cages containing wood shaving as bedding material, and maintained in the departmental animal house at 26 ± 2 °C and 44–55% relative humidity with a natural light/dark cycle. All animals had *ad libitum* access to food (rodent diet) and water. After initial duration of 12 h fast, the animals were rendered diabetic by a single intraperitoneal administration of NA in normal saline at a dose of 230 mg/kg body weight, that was followed by freshly prepared solution of STZ in 0.1 M citrate buffer (pH 4.5) at a dose of 60 mg/kg body. The animals were allowed to drink 5% glucose solution overnight to prevent STZ-NA-induced hypoglycemia.[44] The rats were considered as diabetic if their blood glucose levels were above 250 mg/dL on the 3rd day after STZ-NA injection. The rats were divided into four groups of six animals in each group. Control animals received normal saline (Group I). Diabetic rats received STZ-NA injection (Group II). Diabetic rats orally fed with standard (Pioglitazone) and test drugs (**VIe** and **VIf**) as 0.25% suspension in carboxymethyl cellulose at a dose of 36 mg/kg for 15 days (Groups III and IV). Blood glucose levels were determined from blood obtained from tail vein of the animal on Days 1, 3, 7 and 15, using glucose meter (ACCu-Chek active, Roche, Diagnostics USA).

Biochemical Determinations

After pharmacological screening for antidiabetic activity, the animals were subjected to overnight fasting. Blood samples were collected from retro-orbital region under light anaesthesia. Total Hb was estimated by cyanomethaemoglobin method,[45] whereas HbA1c was estimated from whole blood using commercially available kits (ERBA Diagnostics Inc, Accurex Biomedical Pvt. Ltd., Coral clinical systems, India). TG concentration was determined by GPO-POD enzymatic-colorimetric method.[46] TC level was measured by the end point, CHOD-POD colorimetric methods.[47] HDL-C was assayed as previously reported.[48] VLDL-C and LDL-C in plasma were calculated according to the Friedewald formula: VLDL-C = TG/5; LDL-C = TC-(HDL-C + VLDL-C).[49] Levels of serum urea, uric acid, and creatinine were assessed using commercially available kits.[50]

Histopathological Study

Rats were sacrificed under light anesthesia using diethylether. Pancreas and liver tissues were dissected, washed in ice cold physiological saline, fixed in a 15% buffered neutral formalin solution and, finally, embedded into paraffin blocks. Then, the tissue was sliced out into sections of 5 µm thickness by a rotator microtome and stained with hematoxylin-eosin. Obtained sections were examined by a Leica DME microscope, and representative photomicrographs were taken by a 7.1 megapixel Canon Power Shot S70 digital camera.

Statistical Analysis

All statistical tests were performed using GraphPad Prism 5.0 software (San Diego, California, USA). Results were expressed as mean ± S.E.M. (standard error of the mean) for six rats in each group. The data was analyzed by one-way analysis of variance (ANOVA) followed by Dunnett's multiple variance test. Differences were considered statistically significant at the levels of $P < 0.05$.

Acknowledgements

This study was supported by the grant "Combattere la resistenza tumorale: piattaforma integrata multidisciplinare per un

This article is protected by copyright. All rights reserved.

Accepted Manuscript

approccio tecnologico innovativo alle oncoterapie - CAMPANIA ONCOTERAPIE" (Project N. B61G18000470007) of Regione Campania (Italy). S.Y. and M.U.M.S. acknowledge UGC for JRF (MUS-JH-12-13-11472) under MANF Scheme. Authors are also thankful to DST-FIST (SR/FST/CSI-242/2012) for NMR facility at Birla Institute of Technology, Mesra and Institute of Life Sciences, Hyderabad, AP, India for providing spectral data

Keywords: Type 2 diabetes • Ferulic acid amides • Peroxiredoxin 1 • Hyperglycemia • Hyperlipidemia

[1] S. E. Kahn, R. L. Hull, K. M. Utzschneider, *Nature* **2006**, *444*, 840-846.

[2] a) N. I. o. Health, *Accessed at diabetes. niddk. nih. gov/dm/pubs/statistics/index. htm* **2008**; b) K. M. Darwish, I. Salama, S. Mostafa, M. S. Gomaa, M. A. Helal, *Eur. J. Med. Chem.* **2016**, *109*, 157-172.

[3] S. A. Paschou, R. D. Leslie, *BMC Med.* **2013**, *11*, 161.

[4] a) H. Hui, G. Tang, V. L. W. Go, *Chin. Med.* **2009**, *4*, 11; b) D. K. Patel, S. K. Prasad, R. Kumar, S. Hemalatha, *Asian Pac. J. of Trop. Biomed.* **2012**, *2*, 320-330.

[5] S. B. Ghatak, S. J. Panchal, *Trends Food Sci. Technol.* **2010**.

[6] a) C. Mancuso, R. Santangelo, *Food Chem. Toxicol.* **2014**, *65*, 185-195; b) H. El-Bassossy, D. Badawy, T. Neamatallah, A. Fahmy, *Chem.-Biol. Interact.* **2016**, *254*, 191-197.

[7] E. Nomura, A. Kashiwada, A. Hosoda, K. Nakamura, H. Morishita, T. Tsuno, H. Taniguchi, *Bioorg. Med. Chem.* **2003**, *11*, 3807-3813.

[8] a) M. Ohnishi, T. Matuo, T. Tsuno, A. Hosoda, E. Nomura, H. Taniguchi, H. Sasaki, H. Morishita, *Biofactors* **2004**, *21*, 315-319; b) M. Balasubashini, R. Rukkumani, P. Viswanathan, V. P. Menon, *Phytother. Res.* **2004**, *18*, 310-314; c) P. K. Prabhakar, R. Prasad, S. Ali, M. Doble, *Phytomedicine* **2013**, *20*, 488-494; d) M. Srinivasan, A. R. Sudheer, V. P. Menon, *J. Clin. Biochem. Nutr.* **2007**, *40*, 92-100; e) C. Mancuso, R. Santangelo, *Food Chem. Toxicol.* **2014**, *65*, 185-195.

[9] a) J. P. Berger, T. E. Akiyama, P. T. Meinke, *Trends Pharmacol. Sci.* **2005**, *26*, 244-251; b) T. M. Willson, M. H. Lambert, S. A. Kliewer, *Annu. rev. Biochem.* **2001**, *70*, 341-367.

[10] a) C. Park, S. Marqusee, *Nat. Methods* **2005**, *2*, 207-212; b) B. Lomenick, R. Hao, N. Jonai, R. M. Chin, M. Aghajan, S. Warburton, J. Wang, R. P. Wu, F. Gomez, J. A. Loo, J. A. Wohlschlegel, T. M. Vondriska, J. Pelletier, H. R. Herschman, J. Clardy, C. F. Clarke, J. Huang, *Proc. Natl. Acad. Sci. U. S. A.* **2009**, *106*, 21984-21989.

[11] Z. Tang, N. Xia, X. Yuan, X. Zhu, G. Xu, S. Cui, T. Zhang, W. Zhang, Y. Zhao, S. Wang, *Biochem. Biophys. Res. Commun.* **2015**, *465*, 670-677.

[12] a) A. Pinelli, C. Godio, A. Laghezza, N. Mitro, G. Fracchiolla, V. Tortorella, A. Lavecchia, E. Novellino, J.-C. Fruchart, B. Staels, *J. Med. Chem.* **2005**, *48*, 5509-5519; b) L. Porcelli, F. Gilardi, A. Laghezza, L. Piemontese, N. Mitro, A. Azzariti, F. Altieri, L. Cervoni, G. Fracchiolla, M. Giudici, *J. Med. Chem.* **2011**, *55*, 37-54.

[13] a) F. Dal Piaz, M. B. Vera Saltos, S. Franceschelli, G. Forte, S. Marzocco, T. Tuccinardi, G. Poli, S. Nejad Ebrahimi, M. Hamburger, N. De Tommasi, *J. Nat. Prod.* **2016**, *79*, 2681-2692; b) M. Vasaturo, R. Cotugno, L. Fiengo, C. Vinegoni, F. Dal Piaz, N. De Tommasi, *Sci. Rep.* **2018**, *8*, 1-13.

[14] A. Trzeciecka, S. Klossowski, M. Bajor, R. Zagozdzon, P. Gaj, A. Muchowicz, A. Malinowska, A. Czerwoniec, J. Barankiewicz, A. Domagala, J. Chlebowska, M. Prochorec-Sobieszek, M. Winiarska, R. Ostaszewski, I. Gwizdalska, J. Golab, D. Nowis, M. Firczuk, *Oncotarget* **2016**, *7*, 1717-1731.

[15] A. Zeida, M. Trujillo, G. Ferrer-Sueta, A. Denicola, D. o. A. Estrin, R. Radi, *Chem. Rev.* **2019**, *119*, 10829-10855.

[16] a) T. A. Halgren, R. B. Murphy, R. A. Friesner, H. S. Beard, L. L. Frye, W. T. Pollard, J. L. Banks, *J. Med. Chem.* **2004**, *47*, 1750-1759; b) R. A. Friesner, J. L. Banks, R. B. Murphy, T. A. Halgren, J. J. Klicic, D. T. Mainz, M. P. Repasky, E. H. Knoll, M. Shelley, J. K. Perry, *J. Med. Chem.* **2004**, *47*, 1739-1749.

[17] S. Hirotsu, Y. Abe, K. Okada, N. Nagahara, H. Hori, T. Nishino, T. Hakoshima, *Proc. Natl. Acad. Sci. U. S. A.* **1999**, *96*, 12333.

[18] X.-J. Shi, L. Ding, W. Zhou, Y. Ji, J. Wang, H. Wang, Y. Ma, G. Jiang, K. Tang, Y. Ke, *Antioxid. Redox Signaling* **2017**, *27*, 73-92.

[19] P. Kwiecińska, E. Taubøll, E. Ł. Gregoraszczuk, *Pharmaco.l Rep.* **2012**, *64*, 157-165.

[20] a) E. S. Bjornsson, *Arch. Toxicol.* **2015**, *89*, 327-334; b) M. J. Gomez-Lechon, L. Tolosa, *Arch. Toxicol.* **2016**, *90*, 2049-2061.

[21] C. R. Gardner, C. T. Walsh, O. Almarsson, *Nat. Rev. Drug Discov.* **2004**, *3*, 926-934.

[22] a) M. P. Gleeson, *J. Med. Chem.* **2008**, *51*, 817-834; b) F. Yoshida, J. G. Topliss, *J. Med. Chem.* **2000**, *43*, 2575-2585.

[23] L. Kellard, M. Engelstein, *JALA: Journal of the Association for Laboratory Automation* **2007**, *12*, 104-109.

[24] B. Davies, T. Morris, *Pharm. Res.* **1993**, *10*, 1093-1095.

[25] D. E. Pires, T. L. Blundell, D. B. Ascher, *J. Med. Chem.* **2015**, *58*, 4066-4072.

[26] S. M. Mauer, M. W. Steffes, D. M. Brown, *Am. J. Med.* **1981**, *70*, 603-612.

[27] M. Aurell, S. BjöRck, *Kidney Int., Suppl.* **1992**.

[28] A. Perkins, K. J. Nelson, D. Parsonage, L. B. Poole, P. A. Karplus, *Trends Biochem. Sci.* **2015**, *40*, 435-445.

[29] a) M. H. Park, M. Jo, Y. R. Kim, C.-K. Lee, J. T. Hong, *Pharmacol. Ther.* **2016**, *163*, 1-23; b) C.-X. Liu, Q.-Q. Yin, H.-C. Zhou, Y.-L. Wu, J.-X. Pu, L. Xia, W. Liu, X. Huang, T. Jiang, M.-X. Wu, *Nat. Chem. Biol.* **2012**, *8*, 486; c) W. Wei, C. Ma, Y. Cao, L. Yang, Z. Huang, D. Qin, Y. Chen, C. Liu, L. Xia, T. Wang, *Oncotarget* **2016**, *7*, 3873; d) H. Zhu, B. Wang, L. Kong, T. An, G. Li, H. Zhou, L. Gong, Z. Zhao, Y. Gong, H. Sun, *Cell Chem. Biol.* **2019**, *26*, 1122-1132.

[30] a) A. A. Al-Masri, E. El Eter, S. Tayel, H. Zamil, *Eur. Rev. Med. Pharmacol. Sci.* **2014**, *18*, 710-716; b) E. El Eter, A. A. Al-Masri, *Braz. J. Med. Biol. Res.* **2015**, *48*, 465-469.

[31] J. S. Stancill, J. T. Happ, K. A. Broniowska, N. Hogg, J. A. Corbett, *Am. J. Physiol.: Regul., Integr. Comp. Physiol.* **2020**, *318*, R1004-R1013.

[32] C.-n. Xia, H.-b. Li, W.-x. Hu, *Bioorg. Med. Chem. Lett.* **2008**, *18*, 6553-6557.

[33] V. N. Badavath, I. Baysal, G. Ucar, S. K. Mondal, B. N. Sinha, V. Jayaprakash, *Arch. Pharm. (Weinheim)* **2016**, *349*, 9-19.

[34] B. Ç. Ergün, T. Çoban, F. K. Onurdag, E. Banoglu, *Arch. Pharmacal Res.* **2011**, *34*, 1251-1261.

[35] E. Nomura, A. Kashiwada, A. Hosoda, K. Nakamura, H. Morishita, T. Tsuno, H. Taniguchi, *Biorg. Med. Chem.* **2003**, *11*, 3807-3813.

[36] E. Raspe, L. Madsen, A. M. Lefebvre, I. Leitersdorf, L. Gelman, J. Peinado-Onsurbe, J. Dallongeville, J. C. Fruchart, R. Berge, B. Staels, *J. Lipid Res.* **1999**, *40*, 2099-2110.

[37] T. Hollon, F. K. Yoshimura, *Anal. Biochem.* **1989**, *182*, 411-418.

[38] M. Tauro, A. Laghezza, F. Loiodice, L. Piemontese, A. Caradonna, D. Capelli, R. Montanari, G. Pochetti, A. Di Pizio, M. Agamennone, C. Campestre, P. Tortorella, *J. Enzyme Inhib. Med. Chem.* **2016**, *31*, 25-37.

[39] M. Vasaturo, L. Fiengo, N. De Tommasi, L. Sabatino, P. Ziccardi, V. Colantuoni, M. Bruno, C. Cerchia, E. Novellino, A. Lupo, A. Lavecchia, F. D. Piaz, *Sci. Rep.* **2017**, *7*, 41273.

[40] W. Fiskus, V. Coothankandaswamy, J. Chen, H. Ma, K. Ha, D. T. Saenz, S. S. Krieger, C. P. Mill, B. Sun, P. Huang, *Cancer Res.* **2016**, *76*, 5467-5478.

[41] a) T. J. Jönsson, L. C. Johnson, W. T. Lowther, *Nature* **2008**, *451*, 98-101; b) T. J. Jönsson, L. C. Johnson, W. T. Lowther, *J. Biol. Chem.* **2009**, *284*, 33305-33310.

[42] J. B. Baell, G. A. Holloway, *J. Med. Chem.* **2010**, *53*, 2719-2740.

[43] D. Lagorce, O. Sperandio, J. B. Baell, M. A. Miteva, B. O. Villoutreix, *Nucleic Acids Res.* **2015**, *43*, W200-W207.

[44] a) S. Nazreen, M. S. Alam, H. Hamid, M. S. Yar, A. Dhulap, P. Alam, M. Pasha, S. Bano, M. M. Alam, S. Haider, *Bioorg. Med. Chem. Lett.* **2014**, *24*, 3034-3042; b) N. Altan, Ş. Yigit, E. Elmali, E. Malhatun, S. Rota, N. Kiliç, *General Pharmacology: The Vascular System* **1997**, *28*, 795-796.

[45] D. L. Drabkin, J. H. Austin, *J. Biol. Chem.* **1932**, *98*, 719-733.

[46] M. McGowan, J. D. Artiss, D. R. Strandbergh, B. Zak, *Clin. Chem.* **1983**, *29*, 538-542.

[47] P. Roeschlau, E. Bernt, W. Gruber, *Zeitschrift fur klinische Chemie und klinische Biochemie* **1974**, *12*, 226-226.

[48] T. H. Grove, *Clin. Chem.* **1979**, *25*, 560-564.

[49] W. T. Friedewald, R. I. Levy, D. S. Fredrickson, *Clin. Chem.* **1972**, *18*, 499-502.

[50] M. Jaffé, *Zeitschrift für physiologische Chemie* **1886**, *10*, 391-400.

Accepted Manuscript

This article is protected by copyright. All rights reserved.

Entry for the Table of Contents

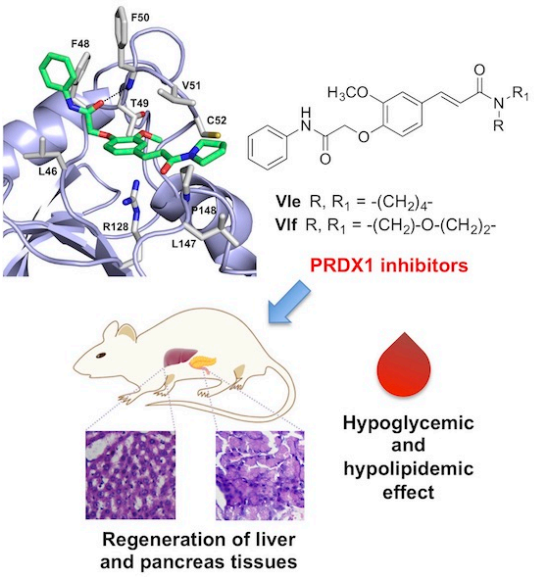

Ferulic acid derivatives (FAAs) **VIe** and **VIf** displayed inhibitory activity against peroxiredoxin 1 (PRDX1), an antioxidant protein implied in the development of T2DM. **VIe** and **VIf** improved hyperglycemia and hyperlipidemia in STZ-NA-induced diabetic rats, preserved the normal histological appearance of liver and recuperated the structural integrity of pancreatic islet β-cells and tissues. Therefore, FAAs represent new promising antidiabetic agents.

WILEY-VCH

Accepted Manuscript

This article is protected by copyright. All rights reserved.